Mineralogical Magazine, April 2017, Vol. 81(2), pp. 217–250

The *REE*- and HFSE-bearing phases in the Itatiaia alkaline complex (Brazil) and geochemical evolution of feldspar-rich felsic melts

Leone Melluso[1,*], Vincenza Guarino[1], Michele Lustrino[2,3], Vincenzo Morra[1] and Roberto de' Gennaro[1]

[1] Dipartimento di Scienze della Terra, dell'Ambiente e delle Risorse, Università di Napoli Federico II, via Mezzocannone 8, 80134 Napoli, Italy
[2] Dipartimento di Scienze della Terra, Università di Roma La Sapienza, P.le Aldo Moro 5, 00185 Roma, Italy
[3] CNR-IGAG c/o Dipartimento di Scienze della Terra, Università di Roma La Sapienza, P.le Aldo Moro 5, 00185 Roma, Italy

[*Received 7 February 2016; Accepted 17 May 2016; Associate Editor: Jason Harvey*]

ABSTRACT

The Late Cretaceous Itatiaia complex is made up of nepheline syenite grading to peralkaline varieties, quartz syenite and granite, emplaced in the metamorphic rocks of the Serra do Mar, SE Brazil. The nepheline syenites are characterized by assemblages with alkali feldspar, nepheline, Fe-Ti oxides, clinopyroxene, amphibole, apatite and titanite, while the peralkaline nepheline syenites have F-disilicates (rinkite, wöhlerite, hiortdahlite, låvenite), britholite and pyrophanite as the accessory phases. The silica-oversaturated rocks have alkali feldspar, plagioclase, quartz, amphibole, clinopyroxene and Fe-Ti oxides; the chevkinite-group minerals are the featured accessory phases and are found with allanite, fluorapatite, fluorite, zircon, thorite, yttrialite, zirconolite, pyrochlore and yttrocolumbite. The major- and trace-element composition of the Itatiaia rocks have variations linked to the amount of accessory phases, have smooth, enriched chondrite-normalized rare-earth element (*REE*) distribution patterns in the least-evolved nepheline syenites and convex patterns in the most-evolved nepheline syenites. The *REE* distribution patterns of the quartz syenites and granites show a typical pattern caused by fractional crystallization of feldspar and amphibole, in an environment characterized by relatively high oxygen fugacity (>NiNiO buffer) and high concentrations of H_2O and F, supporting the crystallization of hydrous phases, fluorite and F-disilicates. The removal of small amounts of titanite in the transition from the least-evolved to the most-evolved nepheline syenites stems from petrogenetic models involving *REE*, and is shown to be a common feature of the magmatic evolution of many other syenitic/ trachytic/ phonolitic complexes of the Serra do Mar and elsewhere.

Keywords: nepheline syenites, quartz-syenites, granites, peralkaline rocks, accessory phases, high-field-strength elements, rare-earth elements, Itatiaia.

Introduction

The Itatiaia igneous complex belongs to the Cretaceous-Cenozoic alkaline province of south-eastern Brazil, which is distributed all around the Paraná Basin (Ulbrich and Gomes, 1981; Sonoki and Garda 1988; Comin-Chiaramonti and Gomes, 2005; Gomes *et al.*, 2011; Motoki *et al.*, 2010; Geraldes *et al.*, 2013; Fig. 1*a*). The alkaline magmatism in southeastern Brazil spans from ~132 to ~58 Ma, with a climax at ~85–90 Ma (Morbidelli *et al.*, 1995; Thompson *et al.*, 1998; Guarino *et al.*, 2013). The earliest intrusions (Anitapolis, Juquiá and Jacupiranga, 132–127 Ma) are coeval with the neighbouring flood tholeiites of the Paraná basin (133 ± 2 Ma; Renne *et al.*, 1992; Turner *et al.*, 1994; Janasi *et al.*, 2011), but the most abundant alkaline activity postdates them by over

* E-mail: melluso@unina.it
https://doi.org/10.1180/minmag.2016.080.122

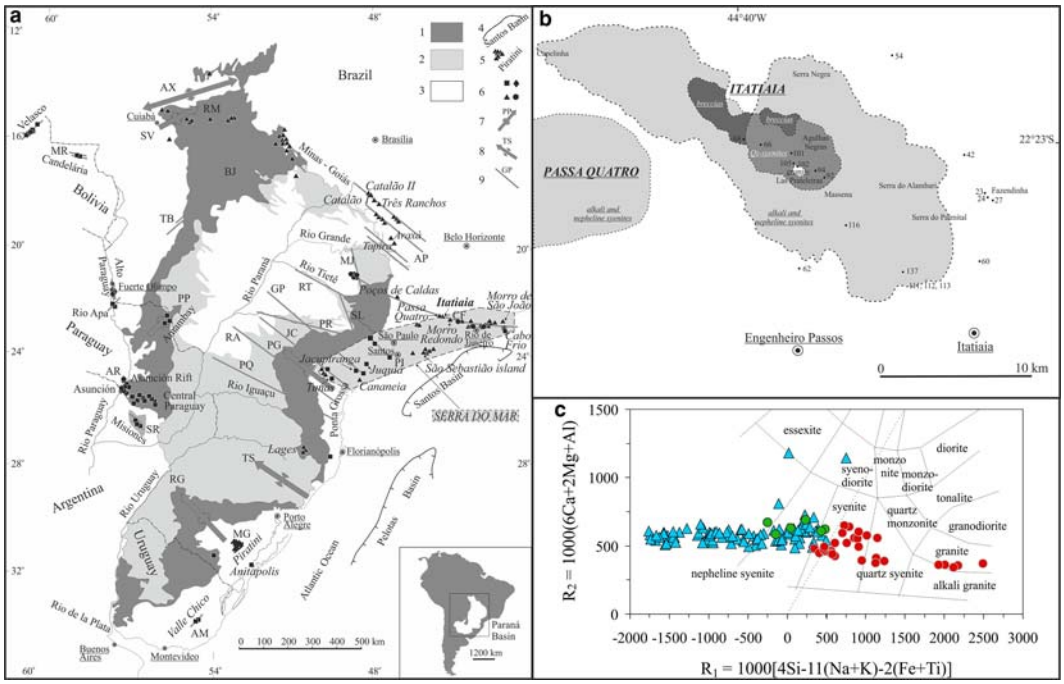

FIG. 1. (*a*) Alkaline provinces of southeastern Brazil and their relationships with major structural features (modified after Guarino *et al.*, 2012): (1) Late Ordovician to Early Cretaceous Paraná Basin; (2) Early Cretaceous tholeiitic lava flows; (3) Late Cretaceous Bauru Basin; (4) Offshore marginal basins; (5) Alkaline provinces; (6) Age of alkaline rocks (diamonds: Permian-Triassic; squares: Early Cretaceous; triangles: Late Cretaceous; circles: Paleogene); (7) Axes of main arcs (AX, Alto Xingu; SV, São Vicente; BJ, Bom Jardim de Goiás; PG, Ponta Grossa; RG, Rio Grande; PP, Ponta Porã); (8) Torres Syncline; (9) Major fracture zones, in part deep lithospheric faults (Rifts: MR, Mercedes; RM, Rio das Mortes; MG, Moirão; SR, Santa Rosa; AR, Asunción; Lineaments: TB, Transbrasiliano; AP, Alto Paranaíba; MJ, Moji-Guaçu; CF, Cabo Frio; RT, Rio Tietê; SL, São Carlos-Leme; PR, Paranapanema; PI, Piedade; GP, Guapiara; JC, São Jerônimo-Curiúva; RA, Rio Alonzo; PQ, Rio Piquiri; AM, Santa Lucia-Aiguá-Merin). Insets: (*b*) Sketch map of the Itatiaia intrusion [modified after Penalva (1967) and Brotzu *et al.* (1997)] with location of the studied samples. (*c*) R_1-R_2 classification diagram (De La Roche *et al.*, 1980). Symbols: quartz-syenites and granites = red; nepheline syenites = blue; corundum-bearing and corundum-normative syenites = green.

40–50 M.y. The youngest alkaline rocks (Late Cretaceous-Eocene) are distributed mainly along the western and southern borders of the São Francisco Craton, in the Ribeira and Brasilia Proterozoic mobile belts, respectively (Ulbrich and Gomes, 1981; Brotzu *et al.*, 2005; Guarino *et al.*, 2013) and are not associated with coeval tholeiitic magmatism, excluding the Cabo Frio area, at the end of the Rio de Janeiro coastline (Bennio *et al.*, 2002, 2003).

The igneous rocks of the Alto Paranaíba and Serra do Mar have compositions ranging from strongly ultrabasic (carbonatites, kimberlites and kamafugites) to silicic (SiO_2 up to 72 wt.%), showing mildly sodic- to- ultrapotassic affinity (Valença, 1980; Ulbrich and Gomes, 1981; Bellieni *et al.*, 1990; Morbidelli *et al.*, 1995; Thompson *et al.*, 1998; Brotzu *et al.*, 2005; Melluso *et al.*, 2008; Azzone *et al.*, 2009; Guarino *et al.*, 2013). In contrast, the Cretaceous alkaline rocks cropping-out in southernmost Brazil and Uruguay (e.g. Tunas, Banhadão, Cananeia, Piratini, Valle Chico/Mariscala) have mostly transitional to sodic affinity, with rare potassic and even rarer ultra-potassic compositions (Barbieri *et al.*, 1987; Gomes *et al.*, 1987, 2011; Morbidelli *et al.*, 1995; Lustrino *et al.*, 2005; Spinelli and Gomes, 2008). Alkaline, or mixed alkaline-subalkaline intrusions, broadly related to the Paraná-Etendeka magmatic cycle are also well known in southern Africa

https://doi.org/10.1180/minmag.2016.080.122 Published online by Cambridge University Press

(Angola, Namibia), and are represented by Brandberg, Erongo, Messum, Okenyenya and many others (cf. Lanyon and le Roex, 1995; Harris *et al.*, 1999; Schmitt *et al.*, 2000).

On the São Paulo-Rio de Janeiro coastline and in its hinterland, the alkaline activity is now mostly eroded to sub-volcanic intrusion level. The most abundant lithologies found in the various intrusions are potassic syenites, with subordinate mafic-ultramafic-intermediate intrusive rocks (e.g. clinopyroxenites, alkali gabbros, theralites, essexites, shonkinites and malignites). Mafic alkaline dyke swarms (mostly basanites and alkali basalts, plus rarer camptonites and foidites), together with subordinate felsic differentiates (tephritic phonolites, trachyandesites, trachytes and phonolites) cross-cut some alkaline complexes and the crystalline basement (e.g. Brotzu *et al.*, 1989, 2005; Sichel *et al.*, 2012; Motoki *et al.*, 2015).

The accessory phase mineralogy of the Brazilian syenites of Late Cretaceous age is very poorly known, though essential for a better understanding of the late-stage petrogenesis of the abundant, highly evolved felsic rocks, and their potential repository of *REE* and high-field-strength elements (HFSE) after extensive feldspar removal. This work follows Brotzu *et al.* (1997, 2005) presenting an improved set of bulk-rock and mineral compositional data for the main lithologies of Itatiaia, with specific reference to the accessory phases of the peralkaline syenites and granites. The genetic relationships with the evolved lithotypes of the Serra do Mar Province are highlighted.

Geological setting

The alkaline massif of Itatiaia is a Late Cretaceous intrusion (~72 Ma; Brotzu *et al.*, 1997 and references therein) located in the Serra da Mantiqueira, near the complexes of Passa Quatro and Morro Redondo (Fig. 1*b*), and southeast of the Poços de Caldas nepheline syenite-phonolite complex (Lustrino *et al*., 2003). The Itatiaia massif crops out for ~220 km^2, and reaches a height of 2787 m (Agulhas Negras), with a roughly ellipsoidal NW-SE trending shape, parallel to the regional tectonic lineaments of the Ribeira Belt (Penalva, 1967; Riccomini *et al.*, 2005). The external part of the complex is formed by an association of several plug- or dyke-type intrusions of syenites and nepheline syenites. Some intrusions may have been displaced radially by younger ones and by faults related to the regional tectonic system.

The inner part of the complex is formed by several small quartz-syenitic-to-granitic intrusions, and a sequence of magmatic breccias, with clasts petrographically similar to the syenites and volcanic/subvolcanic clasts of trachytic composition (e.g. Pires *et al.*, 2014). Field relationships and annular geomorphological features indicate clearly that the quartz syenites and granites post-date the nepheline syenites (Penalva, 1967). The presence of breccia deposits also indicates that the currently exposed erosion level cannot be much deeper from the actual (upper) level of intrusion of the complex. The external limits of the intrusion are only partially known, due to abundant forestation and poor outcrops, but they are very probably more extensive than those reported by Penalva (1967; Fig. 1*b*).

Analytical techniques

The samples investigated in this study are concentrated in the centre and south-eastern part of the intrusion (Fig. 1*b*). New bulk-rock major- and trace-element analyses of the Itatiaia rocks have been obtained by X-ray fluorescence at Naples, using a Panalytical Axios instrument and by inductively coupled plasma mass spectrometry at Ancaster, Ontario (http://www.actlabs.com for reference standards and analytical techniques).

New mineral compositions (more than 1000 analyses) on samples of the dataset of Brotzu *et al.* (1997), with specific focus on peralkaline syenites and granites, were obtained with an Energy Dispersive Spectrometer at Di.S.T.A.R., University of Napoli Federico II (a JEOL JSM-5310 microscope and an Oxford Instruments Microanalysis Unit, equipped with an INCA X-act detector and operating at 15 kV primary beam voltage, 50–100 mA filament current, variable spot size, from 30,000 to 200,000x magnification, 20 mm WD and 50 s net acquisition real time). Measurements were made with an INCA X-stream pulse processor and with *Energy* software. *Energy* uses the *XPP* matrix correction scheme, developed by Pouchou and Pichoir (1991), and the *Pulse Pile up* correction. The quant optimization is carried out using cobalt (FWHM - full width at half maximum peak height - of the strobed zero = 60–65 eV). The following standards were used for calibration: diopside (Ca), San Carlos olivine (Mg), anorthoclase (Al, Si), albite (Na), rutile (Ti), fayalite (Fe), Cr_2O_3 (Cr), rhodonite (Mn), orthoclase (K), apatite (P), fluorite (F), barite (Ba), strontianite (Sr), zircon (Zr, Hf), synthetic Smithsonian orthophosphates (*REE*, Y,

https://doi.org/10.1180/minmag.2016.080.122 Published online by Cambridge University Press

Sc), pure vanadium, niobium and tantalum (V, Nb, Ta), Corning glass (Th and U), sphalerite (S, Zn), sodium chloride (Cl) and pollucite (Cs). The *K*α, *L*α, *L*β, or *M*α lines were used for calibration, according to the element. Back-scattered electron (BSE) images were obtained with the same instrument (see Melluso *et al.*, 2010, 2014*b* for details). Brotzu *et al.* (1997) used mineral compositions obtained with a CAMECA SX50 at CNR of Padua.

Petrography and mineralogy

The rocks in this study are nepheline syenites, quartz syenites and granites, with a few very fine-grained dyke equivalents (phonolites; Fig. 1*c*). The bulk-rock compositions are reported in Table 1, a synopsis of the assemblages found in the thin sections are reported in Table 2, and representative images of the main accessory phases are reported in Figs 2 and 3.

Rock types

The Itatiaia intrusive rocks are nepheline syenites with variable modal nepheline (12–36 vol.%), quartz syenites (with modal quartz) and granites. About 40% of the nepheline syenites have P.I. (Peralkaline Index = molar(Na + K)/Al) > 1 and should be classified as peralkaline (Supplementary Fig. 1 – supplementary figures have been deposited with the Principal Editor of *Mineralogical Magazine* and are available from http://www.minersoc.org/pages/e_journals/dep_mat_mm.html), even though only a few samples have P.I. > 1.1. The R1-R2 diagram for intrusive rocks (De La Roche *et al.*, 1980; Fig. 1*c*) takes into consideration a larger number of major oxides as classification parameters when compared to the TAS diagram (le Maitre, 2002). According to the R1-R2 diagram, the Itatiaia rocks form a continuous spectrum from nepheline to quartz syenite and granite fields, straddling the SiO_2-saturation boundary. This is also shown in the Petrogeny Residua's System (SiO_2-nepheline-kalsilite), where the nepheline syenites trend towards the phonolitic minimum, while the silica-oversaturated samples trend towards the rhyolite minimum, but without reaching it (Fig. 4).

The dykes cross-cutting the intrusion outside the central core are mostly phonolites. The breccia deposits at the top of the sequence also host quartz-normative trachytic clasts. Brotzu *et al.* (1997) also distinguished corundum-bearing and corundum-normative syenites (normative C up to ~4.1%). We will maintain this subdivision as three major groups, which is very evident in the Petrogeny Residua's System (Fig. 4*b*), though most corundum-normative syenites cannot be distinguished easily from nepheline syenites from a major and trace element point of view.

Mineralogy

The compositions of Itatiaia minerals are reported in Tables 2 to 6 and Supplementary Tables 1 to 12 (Supplementary information has been deposited with the Principal Editor of *Mineralogical Magazine* and is available from http://www.minersoc.org/pages/e_journals/dep_mat_mm.html). The rock-forming minerals at Itatiaia are feldspars ± feldspathoids ± quartz, with mafic phases being confined to minor modal amounts. The composition of plagioclase, alkali feldspar, nepheline and other feldspathoids is reported in Supplementary Table 1. There is no evidence for hyperagpaitic mineral assemblages, which are found mainly in post-magmatic (or even hydrothermal) environments (e.g. Sørensen, 1997; Marks *et al.*, 2008; Andersen *et al.*, 2010; Giehl *et al.*, 2013).

Feldspars

The rare plagioclase in the nepheline syenites is mostly andesine and oligoclase, with rare nearly pure albite ($An_{0–34}$–$Ab_{64–99}$–$Or_{0–2}$). The quartz-bearing rocks have similar plagioclase ($An_{0–38}$–$Ab_{57–98}$–$Or_{0–20}$). Alkali feldspar is dominant in both nepheline syenites ($An_{0–4}$–$Ab_{0–90}$–$Or_{10–97}$) and silica-oversaturated rocks ($An_{0–6}$–$Ab_{0–96}$–$Or_{0–97}$). This phase is commonly turbid and with perthitic exsolution lamellae (Fig. 2). The corundum-bearing syenites have andesine ($An_{35–40}$–$Ab_{58–64}$–Or_1) and potassic alkali feldspar (An_1–$Ab_{17–24}$–$Or_{75–82}$). The concentrations of Ba and Sr are always low (<0.3 wt.% BaO and <1.2 wt.% SrO).

Feldspathoids

Nepheline is the main feldspathoid, and is usually interstitial to alkali feldspar, although in many nepheline syenites it is euhedral. It is characterized by a slight silica-excess (expressed as quartz content in the nepheline-kalsilite-silica diagram of Fig. 4), variable CaO (0–2.1 wt.% CaO) and with a Na/(Na + K) ratio varying from 0.77 to 0.84. The nepheline composition plots around the Morozewicz-Buerger compositions (Fig. 4),

https://doi.org/10.1180/minmag.2016.080.122 Published online by Cambridge University Press

TABLE 1. Major- and trace-element compositions of the Itatiaia rocks.

	ne-bearing	ne-bearing	ne-bearing	ne-bearing	ne-bearing	ne-bearing	ne-bearing	ne-bearing	ne-bearing	ne-bearing
	IT116	IT54	IT113	IT137	IT111	IT112	IT23	IT60	IT24	IT62
	A	A	A	A	A	A	A	A	A	A-phon
Method*	ICP-OES	ICP-OES	ICP-OES	ICP-OES	ICP-OES	ICP-OES	ICP-OES	ICP-OES	ICP-OES	XRF
SiO_2(wt.%)	60.3	60.8	57.1	56.5	53.8	55.5	55.5	56.1	56.4	56.9
TiO_2	0.92	0.63	0.62	0.50	0.44	0.29	0.20	0.50	0.23	0.31
Al_2O_3	17.3	19.3	21.6	21.7	21.5	21.1	21.4	22.4	21.4	21.0
Fe_2O_3	3.30	2.69	2.50	2.55	2.45	2.58	2.64	1.82	3.28	3.20
MnO	0.28	0.23	0.18	0.20	0.19	0.24	0.24	0.16	0.35	0.36
MgO	0.68	0.39	0.30	0.26	0.21	0.21	0.15	0.11	0.09	0.03
CaO	1.94	0.85	1.49	1.62	1.32	1.43	0.90	1.11	0.99	0.96
Na_2O	6.68	7.68	7.30	6.29	7.10	8.47	8.63	8.25	9.08	9.81
K_2O	6.85	6.73	7.38	8.20	9.81	7.81	7.10	7.80	6.97	7.49
P_2O_5	0.19	0.10	0.06	0.07	0.05	0.03	0.02	0.02	0.01	0.01
LOI	0.80	1.10	0.46	0.72	0.91	1.33	1.98	1.57	1.22	
Total	99.3	100.5	98.9	98.5	97.7	99.0	98.8	99.8	100.0	100.0
Trace elements										
Method*	ICP-MS	ICP-MS	ICP-MS	ICP-MS	ICP-MS	ICP-MS	ICP-MS	ICP-MS	ICP-MS	XRF
Sc (ppm)	4	1	1							
Be	3	5	2	8	5	6	7	3	10	
V	35	22	21	39	29	31	23	14	31	20
Cr		110				30				
Zn	130	130	80	140	130	280	170	100	300	237
Ga	26	29	25	34	32	35	38	31	50	
Ge	3	2	2	2	2	2	2	2	2	
Rb	251	191	131	136	235	163	156	170	175	190
Sr	289	87	40	2341	611	817	175	21	260	39
Y	65	53	43	31	27	28	18	46	33	56
Zr	535	635	399	851	705	893	815	541	1576	1680
Nb	253	178	257	261	251	231	198	283	351	422
Mo	11	7	2	8	12	6				
Ag	4	3	3	6	5	5	6	5		
Sn	5	4	6	2	2	3	3	3	2	
Cs	2	3	1	3	2	2	3	1	2	
Ba	96	26	12	657	52	24	7	5		13
La	237	335	355	230	242	223	179	352	267	224

(continued)

TABLE 1. (*contd.*)

Method*	ne-bearing IT116 A ICP-OES	ne-bearing IT54 A ICP-OES	ne-bearing IT113 A ICP-OES	ne-bearing IT137 A ICP-OES	ne-bearing IT111 A ICP-OES	ne-bearing IT112 A ICP-OES	ne-bearing IT23 A ICP-OES	ne-bearing IT60 A ICP-OES	ne-bearing IT24 A ICP-OES	ne-bearing IT62 A-phon XRF
Ce	549	591	630	361	371	329	227	605	324	371
Pr	70	56	58	31	30	25	15	53	20	
Nd	260	189	153	85	76	57	31	129	40	62
Sm	38.2	25.6	15.1	9.5	7.9	5.5	2.9	13.8	3.6	
Eu	4.7	3.1	1.9	2.7	2.0	1.4	0.7	2.5	0.9	
Gd	22.7	18.7	11.2	5.6	6.4	4.3	2.8	9.3	2.3	
Tb	3.1	2.4	1.5	0.9	0.9	0.7	0.4	1.5	0.5	
Dy	15.2	11.9	8.1	5.1	4.4	4.1	2.5	8.6	3.6	
Ho	2.6	2.1	1.6	1.1	1.0	0.9	0.6	1.7	0.9	
Er	6.5	5.5	4.5	3.3	2.8	3.1	1.9	4.6	3.3	
Tm	0.9	0.8	0.6	0.5	0.5	0.5	0.3	0.6	0.7	
Yb	5.0	4.6	3.5	3.5	2.8	3.4	2.4	3.8	4.9	
Lu	0.7	0.7	0.5	0.5	0.5	0.5	0.4	0.6	0.7	
Hf	14.2	15.0	11.4	16.0	13.4	15.7	15.2	13.1	29.2	
Ta	17.3	10.8	20.8	11.1	11.0	7.0	5.9	21.1	6.2	
W	4.0	2.0		5.0	4.0	5.0				
Tl	0.6	0.7	0.3	0.5	0.4		0.4	0.4	0.4	
Pb	11.0	19.0	7.0	29.0	18.0	21.0	31.0	12.0	41.0	
Th	15.8	40.7	36.3	30.8	33.1	26.6	28.8	41.3	44.6	44
U	2.4	7.4	2.2	6.6	6.0	6.5	3.9	5.6	12.6	
Eu/Eu*	0.49	0.43	0.45	1.13	0.85	0.89	0.77	0.67	0.98	
Mg#	32	25	22	19	17	16	12	12	6	2

(continued)

TABLE 1. (*Contd.*)

	ne-bearing IT134 A	ne-bearing IT27 A	c-bearing IT42 C	qz-bearing IT66 Q	qz-bearing IT68 Q	qz-bearing IT94 Q	qz-bearing IT101 Q	qz-bearing IT92 Q	qz-bearing IT105 Q	qz-bearing IT102 Q
Method*	XRF	XRF	ICP-OES	ICP-OES	ICP-OES	ICP-OES	ICP-OES	XRF	ICP-OES	ICP-OES
SiO_2 (wt.%)	57.6	54.2	56.2	62.1	65.2	66.6	65.2	65.1	68.3	72.0
TiO_2	0.54	0.43	0.46	0.87	0.72	0.53	0.59	0.64	0.35	0.22
Al_2O_3	21.2	21.7	23.8	17.0	16.6	16.7	16.3	17.7	14.6	13.5
Fe_2O_3	2.36	3.74	2.89	3.80	3.16	2.34	2.81	2.32	2.56	2.05
MnO	0.14	0.29	0.24	0.15	0.14	0.26	0.42	0.13	0.26	0.21
MgO	0.03	0.01	0.32	0.77	0.66	0.27	0.27	0.23	0.22	0.15
CaO	1.61	1.66	2.22	2.30	1.83	0.60	0.62	0.62	0.60	0.41
Na_2O	7.78	10.11	4.30	4.68	4.89	5.78	5.47	6.40	5.49	4.13
K_2O	8.51	7.61	8.08	6.04	6.11	6.22	5.66	6.62	5.18	5.43
P_2O_5	0.09	0.04	0.05	0.37	0.23	0.09	0.10	0.14	0.02	0.04
LOI			0.50	0.96	0.62	0.23	0.82		1.69	1.56
Total	99.8	99.8	99.0	99.0	100.2	99.6	98.2	99.9	99.2	99.7
Trace elements										
Method*	XRF	XRF	ICP-MS	ICP-MS	ICP-MS	ICP-MS	ICP-MS	XRF	ICP-MS	ICP-MS
Sc (ppm)				4	3	6	5	7	4	2
Be			5	3	5	3	6		11	7
V	6		24	27	24	8	7		7	6
Cr										
Zn			200	90	80	90	190		150	160
Ga			33	19	25	24	23		27	26
Ge			2	2	2	3	2		2	2
Rb	185	115	115	142	183	168	259	154	305	372
Sr	499	1746	378	1423	1039	16	20	12	17	30
Y	26	37	40	33	34	33	58	38	67	52
Zr	536	1070	519	352	519	846	929	319	988	400
Nb	181	288	152	104	136	124	193	95	287	186
Mo			34	2	4	7	10		2	4
Ag			3	2	4	6	6		8	3
Sn			3	4	4	4	6		8	10
Cs			1	1	2	1	1		1	3
Ba	91	89	103	1225	812	14	17	14	11	27
La	138	281	315	91	109	179	140	142	146	126

(continued)

TABLE 1. (*contd.*)

Method*	ne-bearing IT134 A XRF	ne-bearing IT27 A XRF	c-bearing IT42 C ICP-OES	qz-bearing IT66 Q ICP-OES	qz-bearing IT68 Q ICP-OES	qz-bearing IT94 Q ICP-OES	qz-bearing IT101 Q ICP-OES	qz-bearing IT92 Q XRF	qz-bearing IT105 Q ICP-OES	qz-bearing IT102 Q ICP-OES
Ce	246	403	572	182	211	339	268	309	293	257
Pr			56	21	24	36	29		31	25
Nd			163	78	84	121	100		97	82
Sm			18.2	12.2	12.7	15.6	15.2		15.8	14.2
Eu			4.0	4.0	3.1	1.1	1.6		0.8	0.4
Gd			12.9	8.7	8.4	10.6	11.9		10.8	11.7
Tb			1.6	1.2	1.2	1.3	1.9		1.9	1.8
Dy			8.1	6.2	6.5	6.6	10.8		12.0	10.3
Ho			1.5	1.2	1.3	1.3	2.0		2.5	2.0
Er			3.9	3.2	3.6	3.7	5.9		7.7	5.9
Tm			0.5	0.5	0.6	0.6	0.9		1.2	1.0
Yb			3.1	2.8	3.7	3.6	6.3		8.7	6.6
Lu			0.5	0.5	0.6	0.6	1.2		1.5	1.1
Hf			11.1	7.7	12.8	15.8	17.8		29.5	12.8
Ta			13.7	6.8	7.7	6.8	10.6		20.1	15.6
W			5.0	7.0	3.0	1.0	1.0		2.0	16.0
Tl			0.4	0.5	0.5	0.4	0.7		0.7	1.5
Pb			22.0	15.0	14.0	11.0	9.0		16.0	28.0
Th			21.4	13.2	21.5	13.8	18.4		50.1	41.7
U			3.5	4.3	5.2	2.3	5.1		13.0	13.0
Eu/Eu*			0.79	1.18	0.92	0.26	0.36		0.19	0.09
Mg#	3	1	21	32	33	21	18	19	17	15

A: nepheline-bearing rocks; Q: quartz-bearing rocks; C: corundum-bearing syenites; Mg# = 100Mg/(Mg + Fe) molar.
*ICP-OES – inductively coupled plasma optical emission spectrometry; ICP-MS – inductively coupled plasma mass spectrometry; XRF – X-ray fluoresence.

TABLE 2. Synopsis of the mineral assemblages found in the rocks studied. The samples are arranged in decreasing bulk-rock MgO concentration. Other petrochemical parameters are also reported.

	Sample	MgO	D.I.	alk/pl	foids	qz	crn	bt	am	cpx	ttn	rt	psdb	ilm	mt	ap	bri	mnz
A	IT116	0.68	88	x	x			x		x	x				x	x	x	
A	IT54	0.39	93	x	x					x				x				
A	IT113	0.30	88	x	x			x		x	x			x		x	x	
A	IT137	0.26	86	x	x			x			x			x	x			
A	IT111	0.21	90	x	x			x		x						x	x	
A	IT112	0.21	90	x	x					x	x			x				
A	IT23	0.15	91	x	x			x		x				x	x			
A	IT60	0.11	92	x	x			x	x	x	x				x	x	x	
A	IT24	0.09	92	x	x			x		x				x		x	x	
A	IT62	0.03	93	x	x			x		x	x			x			x	
A	IT134	0.03	93	x	x				x		x					x		
A	IT27	0.01	90	x	x			x		x	x					x	x	
C	IT42	0.32	79	x			x	x						x	x			x
Q	IT66	0.77	81	x		x		x		x	x			x	x	x		
Q	IT68	0.66	86	x		x		x	x	x	x			x	x	x		
Q	IT94	0.27	93	x		x		x	x		x	x	x	x	x	x		
Q	IT101	0.27	88	x		x		x	x				x	x	x	x		
Q	IT92	0.23	94	x		x		x	x	x	x			x	x			x
Q	IT105	0.22	91	x		x			x	x		x	x	x	x	x		x
Q	IT102	0.15	92	x		x		x				x	x		x			x

(continued)

TABLE 2. (*contd.*)

									F-disil								
	Sample	chev/perr	all	zrcl	zrn	grt	thor	yttr	CaF_2	wöhl	låv	rink	hiort	pcl	YNb	carb	F-carb	sulf
A	IT116				x				x	x		x						
A	IT54				x				x		x				x			
A	IT113				x				x	x				x				x
A	IT137			x	x													
A	IT111				x				x	x		x	x					
A	IT112								x					x				x
A	IT23				x									x				
A	IT60				x				x	x			x			x		
A	IT24								x								x	
A	IT62				x				x					x				
A	IT134					x												
A	IT27				x					x								x
C	IT42			x	x									x				
Q	IT66	x	x	x														
Q	IT68	x	x+ep		x													
Q	IT94	x			x												x	
Q	IT101	x			bd				x					x				x
Q	IT92	x														x		
Q	IT105				x		x	x	x					x	x	x	x	
Q	IT102	x		x	x+bd		x		x					x	x	x	x	

A: nepheline-bearing rocks; Q: quartz-bearing rocks; C: corundum-bearing syenites. D.I. – Differentiation Index (the sum of normative or + ab + ne + lc + qz + ac + ns). Discriminant phases: qtz and foids; pyrophanite, britholite and Ca-Zr-F disilicates (nepheline-bearing); ilmenite, monazite, chevkinite, allanite, zirconolite?, pseudobrookite?

Key:

alk/pl – alkali feldspar and plagioclase, qz – quartz, crn – corundum, bt – biotite, am – amphibole, cpx – chalcopyrite, ttn – titanite, rt – rutile, psdb – pseudobrookite, ilm – ilmenite, mt – magnetite, ap – apatite, bri – britholite, mnz – monazite. chev/perr – chevkinite/perrierite, all – allanite, zrcl – zirconalite, zrn – zircon, grt – garnet, thor – thorite, yttr – yttrialite, F-disil – F-disilicates, wöhl – wöhlerite, låv – låvenite, rink – rinkite, hiort – hiortdahlite, pcl – , carb – carbonates, F-carb – fluorocarbonates, sulf – sulfides, ep – (other) epidote, bd – baddeleyite.

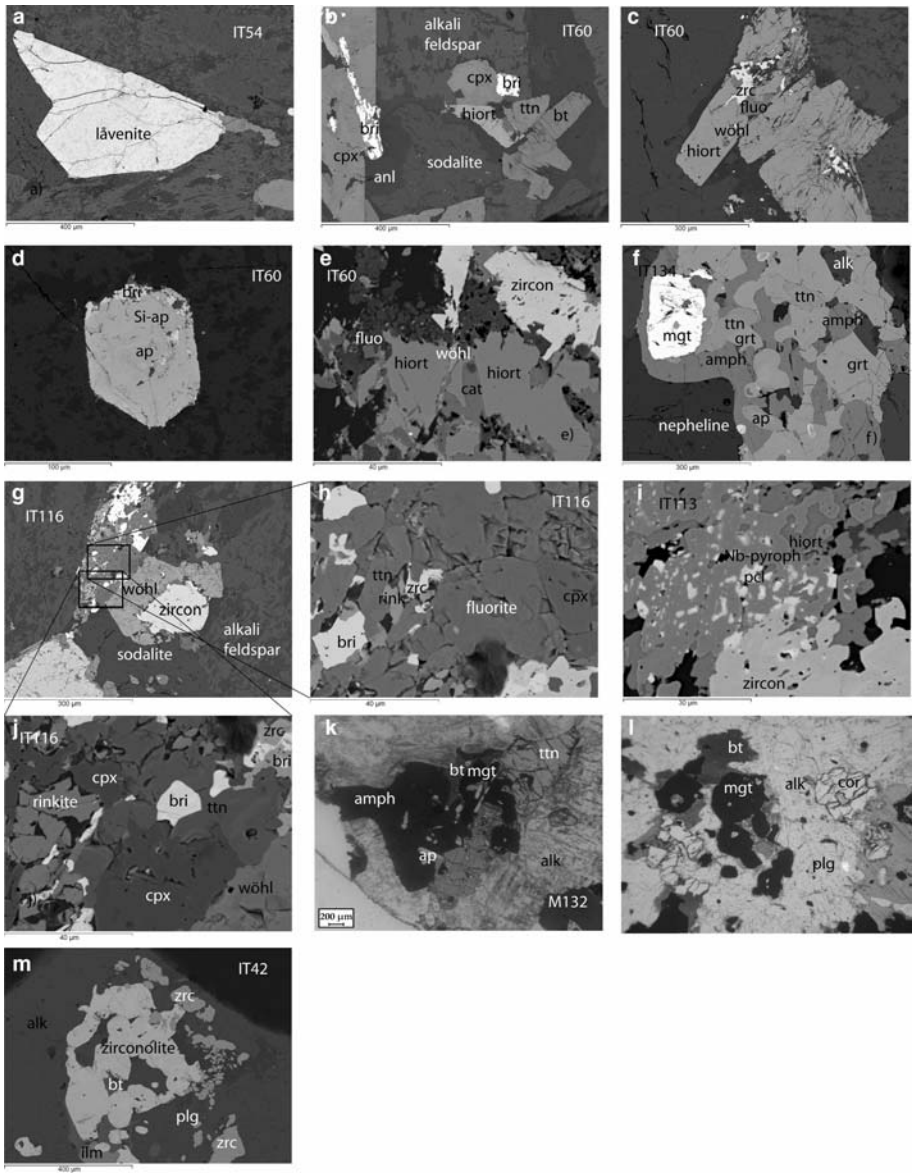

FIG. 2. Back-scattered images of nepheline normative rocks: (*a*) subidiomorphic låvenite, sample IT54; (*b*) idiomorphic britholite, clinopyroxene, titanite and biotite, sample IT60; (*c*) resorbed zircon and fluorite crystals, with a rim of idiomorphic hiortdahlite and small wöhlerite, sample IT60; (*d*) zoning of apatite to britholite, sample IT60; (*e*) zircon and fluorite replaced by hiortdahlite and wöhlerite, with secondary catapleiite, sample IT60; (*f*) early magnetite and titanite, and late amphibole and garnet, sample IT134; (*g*, *h*, *j*) a crystallization-reaction sequence involving zircon and fluorite, with wöhlerite, rinkite, chemically zoned titanite, britholite and felsic phases, sample IT116; (*i*) zircon, pyrophanite, pyrochlore and hiortdahlite, sample IT113; (*k*) aggregate of euhedral/subhedral titanite, amphibole, magnetite, biotite and apatite, sample IT132; (*l*) subhedral corundum grains in the syenite IT42, with biotite, oxides, plagioclase and alkali feldspar; (*m*) aggregate of zirconolite and zircon grains, together with alkali feldspar, plagioclase, ilmenite and biotite, sample IT42.

https://doi.org/10.1180/minmag.2016.080.122 Published online by Cambridge University Press

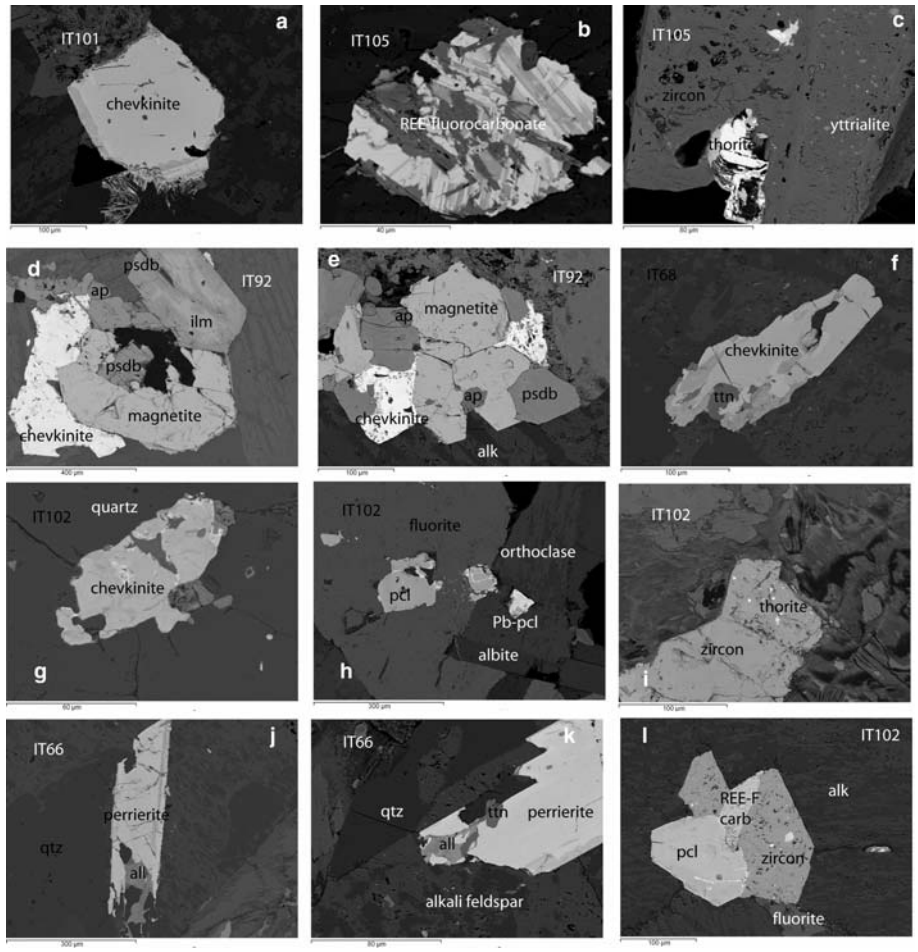

FIG. 3. Back-scattered images of quartz-normative samples: (*a*) idiomorphic chevkinite, sample IT101; (*b*) bastnäsite, sample IT105; (*c*, *i*) zircon with exsolved thorite and yttrialite, samples IT105 and IT102; (*d*, *e*) glomerocrysts of magnetite, ilmenite (with possibly both primary and secondary pseudobrookite), apatite and chevkinite, sample IT92; (*f*) chevkinite and titanite, sample IT68; (*g*) altered chevkinite, granite IT102; (*h*) two pyrochlore types with fluorite, granite IT102; (*j*, *k*) perrierite with secondary allanite, sample IT66; (*l*) intergrowth of *REE*-fluorocarbonate, pyrochlore, zircon and fluorite in sample IT102.

matching those of most other Brazilian syenitic intrusions (e.g. Comin-Chiaramonti and Gomes, 2005; Brotzu *et al.*, 2007) and elsewhere (e.g. Melluso *et al.*, 2012*b* and references therein). Sodalite and nosean are the other rare feldspathoids.

Pyroxenes

The pyroxenes of nepheline syenites range continuously from diopside [$Ca_{47}Mg_{38}Fe_{13}$; Mg# = 77; Mg# = molar Mg/(Mg + Fe^{2+})], through rare hedenbergite, to pure aegirine ($NaFeSi_2O_6$; CaO ~0.17 wt.%; MgO ~0.08 wt.%; Na_2O ~13.0 wt.%; Suppl. Fig. 2; Suppl. Table 2). The pyroxenes of quartz syenites and granites have bimodal compositions, from diopside ($Ca_{45–47}Mg_{41–33}Fe_{14–21}$; Mg# = 66–77; Suppl. Fig. 2; Suppl. Table 2) to very rare aegirine (CaO ~0.23 wt.%; MgO ~0.03 wt.%; Na_2O ~13.4 wt.%; sample IT105). Titanium reaches its highest concentration in an aegirine (TiO_2 = 2.15 wt.%); Zirconium is very low also in the sodic varieties. Manganese increases with Fe in aegirine-augites up to 4.1 wt.% MnO (sample IT60), and then decreases in the most sodic

https://doi.org/10.1180/minmag.2016.080.122 Published online by Cambridge University Press

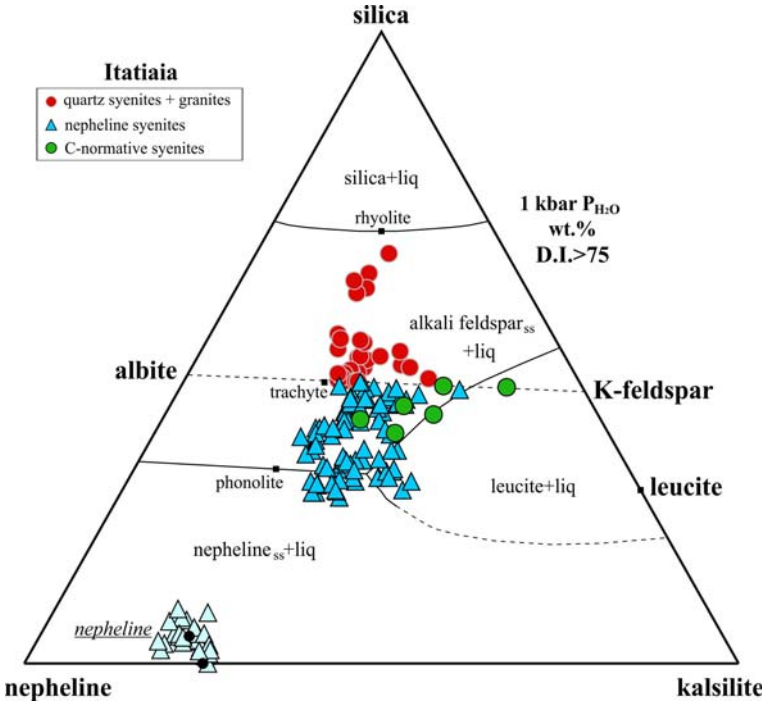

FIG. 4. Nepheline–kalsilite–silica diagram (wt.%) for the rocks of Itatiaia. Univariant lines from Hamilton and Mackenzie (1965) and Gupta (2015). The composition of the nephelines is also reported. Symbols: quartz-syenites and granites = red; nepheline syenites = blue; corundum syenites = green. The Morozevicz and Buerger compositions are the black dots.

and iron-rich pyroxenes (Suppl. Fig. 2). Other interesting features of the Itatiaia pyroxenes are: (1) the crystallization of Na-Fe-rich pyroxene in nepheline syenites is far more abundant than in quartz syenites (Suppl. Fig. 2); and (2) subcalcic pyroxene is absent in the quartz-bearing samples.

Amphibole

Amphibole is the main mafic phase in the quartz syenites and granites, is common in the nepheline syenites, and nearly absent in the peralkaline nepheline syenites (after Giret *et al.*, 1980; Leake *et al.*, 1997; Suppl. Table 3). The amphibole of silica-oversaturated rocks varies continuously from calcic (edenite and actinolite; Mg# up to 83), in the least-evolved quartz syenites, through calcic-sodic (katophorite, ferri-winchite and ferro-richterite) to sodic (riebeckite and arfvedsonite; Mg# down to 6) in granites. With decreasing Mg#, amphibole in silica-oversaturated rocks continuously decreases in Al_2O_3 (from 4.1 to 0.7 wt.%) and CaO (from 12.0 to 0.7 wt.%), and increases in MnO (from 1.1 to 4.5 wt.%) and alkalis (from 1.3 to 9.3 wt.%; Suppl. Fig. 3). The variation of the composition of amphibole in the silica-oversaturated syenites and granites is similar to that observed by Gualda and Vlach (2007) in 580 M.y.-old quartz-bearing syenites and granites of Brazil, by Kempe *et al.* (2015) at Khalzan Buregte (Mongolia) and by Czamanske and Dillet (1988) in silicic peralkaline igneous rocks of Questa, New Mexico. The rare amphibole found in nepheline syenites is both calcic (magnesio-hornblende, hastingsite and sanadagaite) and calcic-sodic (katophorite). It is also characterized by a slightly narrower compositional variation (Mg# = 15–55) compared to the silica-oversaturated counterparts. The TiO_2 concentration varies from 0.3 to 3.0 wt.%. Amphibole (as well as clinopyroxene) is absent in the corundum-bearing syenites.

Micas

Trioctahedral micas mostly plot along the phlogopite-annite join (Suppl. Table 4; Fig. 5). The micas of nepheline syenites have Al_2O_3 from 10.3 to 17.6 wt.% and Mg# from 14 to 63. In the

https://doi.org/10.1180/minmag.2016.080.122 Published online by Cambridge University Press

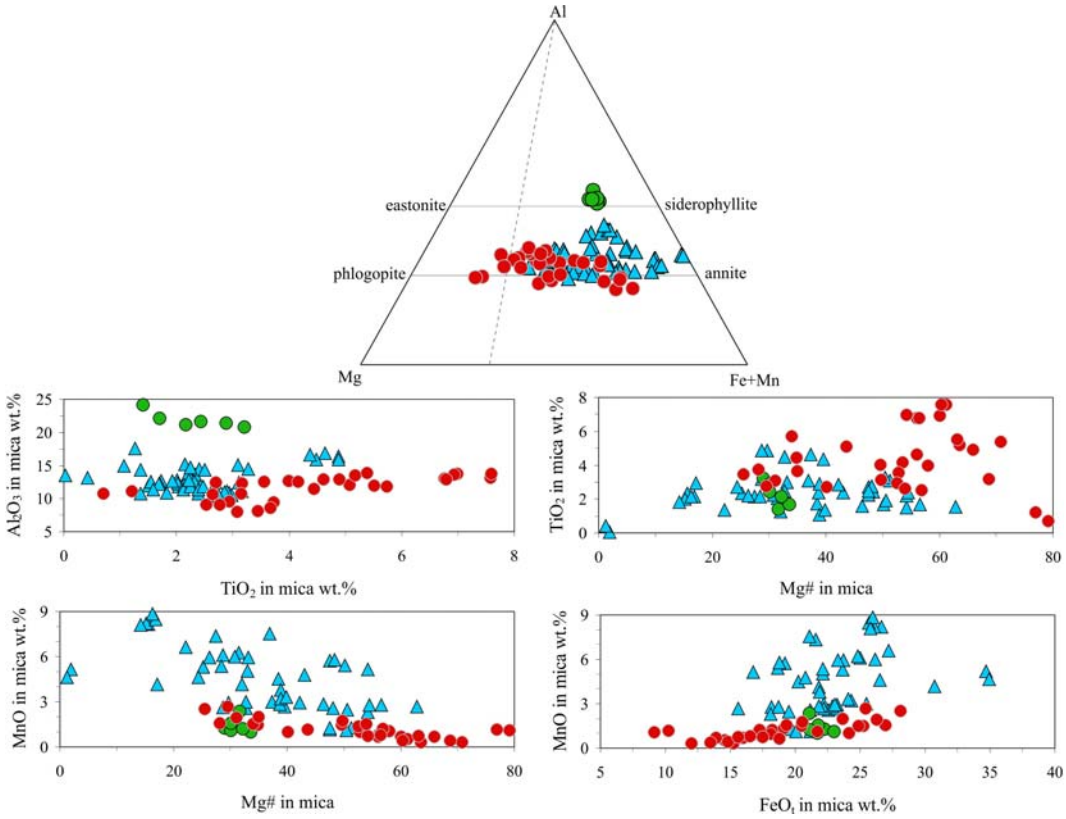

FIG. 5. Mica composition in the Mg-(Fe + Mn)-Al diagram and selected binary diagrams. Symbols: quartz-syenites and granites = red; nepheline syenites = blue; corundum-bearing syenites = green.

same rocks these minerals are also characterized by a significant variation in Mn (1.1-8-8 wt.% MnO) and Ti (0.4–4.9 wt.% TiO_2). Micas in the silica-oversaturated syenites have compositions essentially overlapping those found in nepheline syenites, with Al_2O_3 from 8.1 to 13.8 wt.%, Mg# from 26 to 79 and TiO_2 from 0.7 to 7.6 wt.%, all without any clear intercorrelation. Manganese (0.3–2.7 wt.% MnO) has a clear negative correlation with Mg# (Suppl. Fig. 3) and the Ba concentration is negligible (<0.6 wt.% BaO). The micas of corundum-bearing syenites are characterized by Al-rich compositions, plotting along the siderophyllite-eastonite join (20.8–24.1 wt.% Al_2O_3; Mg# = 29–34).

Opaque oxides

At least five types of 'unexsolved' Fe-Ti oxides occur at Itatiaia: magnetite-ulvöspinel$_{ss}$, ilmenite-haematite-pyrophanite$_{ss}$, pseudobrookite$_{ss}$, rutile$_{ss}$ and Al-spinel (this latter in the corundum-bearing syenites; Suppl. Table 5; Fig. 6*a*).

Spinels are rich in the magnetite component and low in Mg and V, as expected in evolved alkaline rocks. The spinels in the corundum-bearing syenite IT42 are almost pure magnetite and Mn-hercynite (Al_2O_3 = 49.8–53 wt.%; MnO = 4.2–4.5 wt.%; Suppl. Table 5). Zinc is generally low. Rhombohedral oxides show a complete solid solution series between ilmenite ($FeTiO_3$) and pyrophanite ($MnTiO_3$) in the nepheline syenites and in the corundum-bearing syenites (MnO = 11.6–44.6 wt.%; FeO_t = 4.1–36.5 wt.%), with a narrower variation in the quartz syenites and granites (FeO_t = 31–48.7 wt.%; MnO = 1.5–17 wt.%; Fig. 6*b*). The Mn-rich composition of the rhombohedral oxides is another notable feature for the Brazilian alkaline rocks. It somewhat mimics that observed for Zn and Mn by Mitchell and Liferovich (2004) in rhombohedral oxides of syenitic rocks

https://doi.org/10.1180/minmag.2016.080.122 Published online by Cambridge University Press

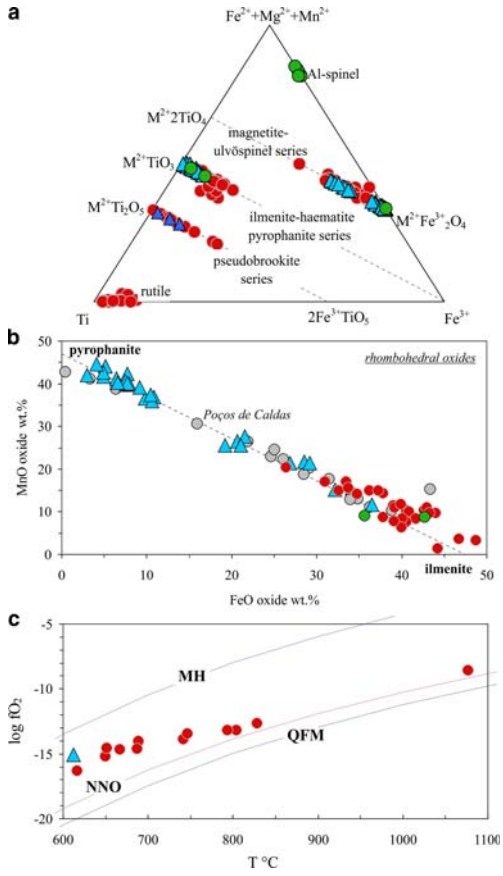

FIG. 6. (*a*) Molar Fe^{3+}-Ti-(Mg + Fe^{2+}-Mn) for the oxides in this study; (*b*) FeO_t–MnO diagram (wt.%) for the rhombohedral oxides. The Poços de Caldas compositions are authors' unpublished data; (*c*) oxygen buffers vs. equilibrium temperature calculated for spinel-rhombohedral phase pairs (cf. Sauerzapf *et al.*, 2008). Symbols: quartz-syenites and granites = red; nepheline syenites = blue; corundum-bearing syenites = green.

from Pilanesberg (South Africa). A similar Mn-Fe variation in ilmenite is found in the peralkaline nepheline syenites of Poços de Caldas (Fig. 6*b*) and, more limited, in syenites of the Los Archipelago (Guinea; Moreau *et al.*, 1996), at Junguni and Mulanje (Malawi; Platt and Woolley, 1988; Woolley and Platt, 1988). Pseudobrookite (classified after Bowles, 1988), a solid solution of $M^{2+}Ti_2O_5$ and $Fe^{3+}_2TiO_5$ (where M is the sum of Fe^{2+}, Mn and Mg), is common in the quartz syenites. Many analyses are not stoichiometric, strongly suggesting secondary hydration processes. The Nb concentration in the Fe-Ti-Mn oxides is widely variable, and tends to be high in ilmenite (up to 3.6 wt.% Nb_2O_5 in nepheline syenites) and pseudobrookite (up to 2.4 wt.% Nb_2O_5 in granites).

Very rare $rutile_{ss}$, sometimes with a notable concentration of tungsten (up to 5.3 wt.% WO_3) and Nb (4–5 wt.% Nb_2O_5), has been analysed in granite IT102 (Suppl. Table 5), with bulk-rock composition of 16 ppm W (Table 1). These high amounts of tungsten are a common feature of mesothermal gold deposits (Clark and Williams-Jones, 2004). Similar compositions have been found in granitic pegmatites elsewhere (e.g. Cerny *et al.*, 2007; Meinhold, 2010).

Chevkinite and perrierite

These rare *REE*-HFSE-bearing silicates [(*LREE*,Sr,Th,Ca)$_4$(Fe^{2+},Mg)$_2$(Ti,Mn,Zr,Nb,Fe^{3+})$Ti_2Si_4O_{22}$, where *LREE* = light rare-earth elements] have been found frequently in quartz syenites and granites (Fig. 3, Suppl. Fig. 4; Table 3; Suppl. Table 6). Chevkinite-(Ce) is a typical accessory in quartz syenites and in granite IT102, whereas perrierite-(Ce) was found together with allanite in the quartz syenite IT66. Chevkinite and perrierite show a significant compositional range, characterized by the inverse variation between FeO and CaO (Fig. 7), though Fe and Ca fill different cationic sites (Baginski and Macdonald, 2013), and by a good correlation between Fe and La_2O_3, with $La_2O_3 + Ce_2O_3 + Nd_2O_3$ reaching concentrations as high as 50 wt.%. Also Al_2O_3, though in low concentrations (0.06–2.63 wt.%), shows a roughly negative relationship with $La_2O_3 + Ce_2O_3 + Nd_2O_3$, whereas the variations in TiO_2 between perrierite and chevkinite are minor. Perrierite-(Ce) has a significantly higher concentration of ZrO_2 than chevkinite-(Ce) (2–4 wt.% *vs.* <2 wt.%); this oxide has a marked negative correlation with REE_2O_3. Perrierite-(Ce) and chevkinite-(Ce) can have a significant concentration of Zn (up to 3.04 wt.% ZnO). The chevkinites of the granite IT102 plot off the main trend, and have a high concentration of Nb_2O_5 (up to 9.6 wt.%) and relatively low FeO and REE_2O_3 (Suppl. Table 6). Several are the possible charge-balancing substitutions in the various sites of these phases (cf. Platt *et al.*, 1987; Macdonald and Belkin, 2002; Vlach and Gualda, 2007; Baginski and Macdonald, 2013; Macdonald *et al.*, 2013*a*), possibly as a response of the bulk-rock changes (degree of magmatic evolution, availability of *REE*, and competition with other phases).

https://doi.org/10.1180/minmag.2016.080.122 Published online by Cambridge University Press

TABLE 3. Representative compositions of chevkinite and perrierite. Oxides and cations are listed following site occupancy, according to their formula.

(wt.%)	Q IT94 chevkinite	Q IT101 chevkinite	Q IT92 chevkinite	Q IT68 chevkinite	Q IT66 perrierite	Q IT66 perrierite	Q IT66 perrierite	Q IT66 perrierite
La_2O_3	14.34	12.79	13.90	15.36	13.58	10.04	9.46	11.00
Ce_2O_3	22.78	22.12	23.33	22.19	21.04	18.43	17.45	19.28
Nd_2O_3	4.38	5.17	6.10	3.49	4.87	6.00	4.92	5.95
Sm_2O_3			0.26					0.65
SrO	0.17	0.73	0.19	0.37				
BaO	0.09	0.55			1.13	0.85	0.62	
ThO_2	0.77	0.48	0.89	0.69	1.02	0.90	0.78	0.50
UO_2		0.53				0.35	0.57	
CaO	3.83	4.57	3.95	4.86	5.29	7.63	7.97	7.68
Na_2O	0.54		0.18					0.00
FeO	11.01	8.74	10.56	9.71	8.62	7.12	7.52	7.69
MnO	0.95	0.39	0.97	0.82	0.35	0.19	0.46	0.27
ZrO_2	0.83	1.25	0.70	1.55	0.45	2.70	3.93	2.81
Nb_2O_5	1.56	1.51	1.40	1.09	0.67	0.63	1.22	0.60
V_2O_3		0.07			0.70	0.26	0.29	
ZnO		2.06			1.92	1.70	1.37	
Y_2O_3	0.66	0.31				0.40	0.52	
TiO_2	17.74	18.76	17.36	18.56	17.18	18.82	18.93	19.59
SiO_2	19.91	19.72	20.09	21.00	20.57	22.48	21.80	21.20
Al_2O_3	0.40	0.54	0.36	1.22	2.17	2.43	2.19	2.19
Total	99.96	100.28	100.24	100.91	99.56	100.94	100.02	100.06
Atoms for 22 oxygens (atoms per formula unit)								
La	1.075	0.952	1.048	1.114	1.002	0.697	0.659	0.773
Ce	1.695	1.635	1.745	1.597	1.540	1.270	1.207	1.345
Nd	0.318	0.373	0.445	0.245	0.348	0.404	0.332	0.405
Sm	0.000	0.000	0.018	0.000	0.000	0.000	0.000	0.043
Sr	0.020	0.086	0.022	0.042	0.000	0.000	0.000	0.000
Ba	0.007	0.043	0.000	0.000	0.089	0.063	0.046	0.000
Th	0.035	0.022	0.042	0.031	0.046	0.039	0.034	0.021
U	0.000	0.024	0.000	0.000	0.000	0.015	0.024	0.000
Ca	0.834	0.989	0.866	1.024	1.133	1.538	1.613	1.568
Na	0.212	0.000	0.072	0.000	0.000	0.000	0.000	0.000
Sum	4.197	4.123	4.258	4.053	4.158	4.025	3.915	4.155
Fe	1.871	1.475	1.805	1.596	1.441	1.121	1.188	1.225
Ti	0.712	0.847	0.668	0.744	0.583	0.664	0.689	0.808
Mn	0.164	0.067	0.167	0.136	0.058	0.030	0.074	0.044
Zr	0.082	0.123	0.070	0.148	0.044	0.247	0.362	0.261
Nb	0.144	0.137	0.129	0.097	0.061	0.054	0.105	0.052
V	0.000	0.011	0.000	0.000	0.112	0.040	0.044	0.000
Zn	0.000	0.307	0.000	0.000	0.284	0.236	0.192	0.000
Y	0.072	0.033	0.000	0.000	0.000	0.040	0.053	0.000
Sum	3.04	3.00	2.84	2.72	2.58	2.43	2.71	2.39
Ti	2	2	2	2	2	2	2	2
Si	4.047	3.980	4.105	4.127	4.114	4.231	4.118	4.039
Al	0.097	0.129	0.086	0.283	0.510	0.539	0.488	0.491
Sum	4.14	4.11	4.19	4.41	4.62	4.77	4.61	4.53

Q: quartz-bearing rocks.

https://doi.org/10.1180/minmag.2016.080.122 Published online by Cambridge University Press

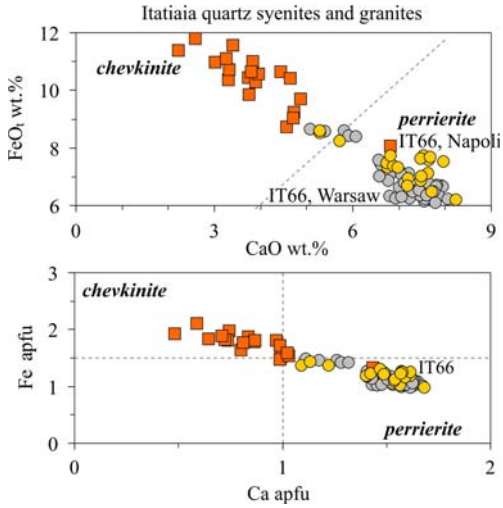

FIG. 7. Chevkinite and perrierite compositions of the quartz bearing rocks in the CaO–FeO diagram (wt.%) of Macdonald and Belkin (2002) and in an Fe–Ca diagram.

Allanite

This mineral $[(Ca,LREE)_2(Al,Fe^{3+},Fe^{2+})_3(SiO_4)(Si_2O_7)O(OH)]$ seems to be a late (possibly subsolidus) phase after chevkinite (Fig. 3*j–k*), and has a limited compositional range (e.g. 28.2–34 wt.% SiO_2, 13.1–17.8 wt.% Al_2O_3, 12.2–22.9 wt.% La_2O_3+Ce_2O_3 + Nd_2O_3). This phase is rich in ZnO (1.5–2.6 wt.%), and has ZrO_2 up to 1.4 wt.% (Table 4; Suppl. Table 6). The abundance of chevkinite and allanite in the Itatiaia silica-oversaturated rocks indicates that these silicates are the most important *REE*-hosting phases, more than monazite. Finally, the presence of allanite in the quartz syenite IT66 indicates that this sample is not peralkaline.

Titanite

Titanite ($CaTiSiO_5$) is very common in most nepheline syenites, typically as very large (several mm) idiomorphic crystals (Fig. 2*k*), but decreases in amount towards the most evolved nepheline syenites. The Nb_2O_5 and ZrO_2 concentrations reach 2.5 and 3.2 wt.%, respectively; similar concentrations are reached by La_2O_3 and Ce_2O_3 (2.0 and 1.7 wt.% respectively). This phase can thus be considered a potential repository of HFSE and *LREE* (Suppl. Table 7). The TiO_2 and Al_2O_3 concentrations have a marked negative correlation, though the ranges in silica-oversaturated and silica-undersaturated rocks are similar. Titanite in granites has lower Nb_2O_5 (up to 2.1 wt.%) and ZrO_2 (up to 2.5 wt.%) concentrations than in the nepheline syenites.

TABLE 4. Representative compositions of allanite. Oxides and cations are listed based on site occupancy, according to their formula.

	Q IT66 allanite	Q IT66 allanite	Q IT66 allanite	Q IT66 allanite	Q IT66 allanite
(wt.%)					
CaO	13.16	13.23	16.21	13.63	11.42
SrO	0.23	0.93	0.68	0.82	0.24
BaO	0.66	0.22		0.51	
La_2O_3	6.97	4.81	3.43	5.24	6.51
Ce_2O_3	9.86	9.33	7.04	9.40	12.26
Nd_2O_3	2.50	3.00	1.72	2.51	4.10
ThO_2		0.51	0.31	0.14	0.13
UO_2	0.56	0.04			0.06
Al_2O_3	15.26	15.62	15.76	15.80	17.78
FeO	14.61	13.47	16.35	13.88	8.58
MnO	0.65	1.21	0.39	0.94	0.49
TiO_2	0.18	0.45	1.25	0.27	0.70
V_2O_3	0.45	0.33		0.08	
ZnO	2.06	1.47	2.06	2.29	1.88
Y_2O_3					0.15
ZrO_2		1.03		1.37	0.50
Nb_2O_5		0.22		0.29	0.35
SiO_2	33.32	32.98	33.98	31.34	32.54
Total	100.44	98.85	99.18	98.51	97.68
Atoms per 8.5 oxygens (apfu)					
Ca	2.630	2.650	3.152	2.773	2.308
Sr	0.025	0.101	0.071	0.090	0.026
Ba	0.048	0.016	0.000	0.038	0.000
La	0.479	0.332	0.230	0.367	0.453
Ce	0.673	0.639	0.467	0.654	0.847
Nd	0.167	0.200	0.111	0.170	0.276
Th	0.000	0.022	0.013	0.006	0.005
U	0.023	0.002	0.000	0.000	0.002
Sum	4.05	3.96	4.04	4.10	3.92
Al	3.354	3.442	3.369	3.538	3.953
Fe	2.278	2.106	2.480	2.204	1.353
Mn	0.102	0.192	0.060	0.152	0.078
Ti	0.025	0.063	0.171	0.039	0.100
V	0.067	0.050	0.000	0.012	0.000
Zn	0.284	0.203	0.276	0.321	0.262
Y	0.000	0.000	0.000	0.000	0.015
Zr	0.000	0.094	0.000	0.127	0.046
Nb	0.000	0.018	0.000	0.025	0.029
Sum	6.11	6.17	6.36	6.42	5.84
Si	6.21	6.17	6.16	5.95	6.14

Q: quartz-bearing rocks.

https://doi.org/10.1180/minmag.2016.080.122 Published online by Cambridge University Press

F-disilicates

This heterogeneous mineral group characterizes the peralkaline nepheline syenites (Fig. 8; Suppl. Fig. 5; Table 5; Suppl. Table 8). They are represented by rinkite [ideally $Na(Na,Ca)_2(Ca,REE)_4(Ti,Nb)(Si_2O_7)_2(O,F)_2$], wöhlerite [ideally $NaCa_2(Zr,Nb)Si_2O_7(O,OH,F)_2$], hiortdahlite [ideally $(Ca,Na,Y)_3(Zr,Ti)Si_2O_7(F,O,OH)_2$] and låvenite [ideally $(Na,Ca)_2(Mn,Fe^{2+})(Zr,Ti,Nb)Si_2O_7(O,OH,F)$]. The association of these phases is not straightforward, as can be seen also in Suppl. Table 8 and in Fig. 8. Wöhlerite has 12.7–15.9 wt.% ZrO_2, 7.8–12.5 wt.%Nb_2O_5, 7–8.7 wt.% Na_2O, 0.7–6.9 wt.% MnO and 23.3–29.4 wt.% CaO, low concentrations of FeO, TiO_2 and REE_2O_3. The rarer hiortdahlite has 12.1–17.9 wt.% ZrO_2, 5.8–9.4 wt.% Na_2O, 27.9–35.4 wt.% CaO and low concentrations of Nb_2O_5, TiO_2, MnO, FeO and REE_2O_3. The even rarer låvenite has 20.8–22.9 wt.% ZrO_2, very low TiO_2, 5.9–6.6 wt.% MnO, 10.3–10.6 wt.% Na_2O and 4.8–5.2 wt.% FeO with minor Nb_2O_5, REE_2O_3 and 14.0–14.9 wt.% CaO. Rinkite is rich in REE_2O_3 (8.9–15.5 wt.% $La_2O_3+Ce_2O_3+Nd_2O_3$), TiO_2 (6.9–9.1 wt.%), Na_2O (6.7–7.7 wt.%) and CaO (26.9–35.5 wt.%), with low concentrations in ZrO_2, Nb_2O_5, FeO + MnO, and SiO_2. Rinkite compositions are typically characterized by relatively low totals (Suppl. Table 8) and, consequently, they plot below the line joining the other phases, suggesting cationic vacancies with respect to the formula normalized to eight Si. These low totals have already been observed by Andersen *et al.* (2013). The compositional characteristics of these phases are best exemplified in the diagrams of Fig. 8 and Suppl. Fig. 5. These phases are clearly distinguished from each other, and the compositional variations suggest that they are solid solutions between different end-members. More generally, there is need of a more stringent chemical classification of these phases, in the absence (and usefulness) of crystallographic determinations made crystal-by-crystal, composition-by-composition (e.g. Atencio *et al.*, 1999; Christiansen *et al.*, 2003*a*,*b*; Chakhmouradian *et al.*, 2008; Andersen *et al.*, 2013; Melluso *et al.*, 2014*b*).

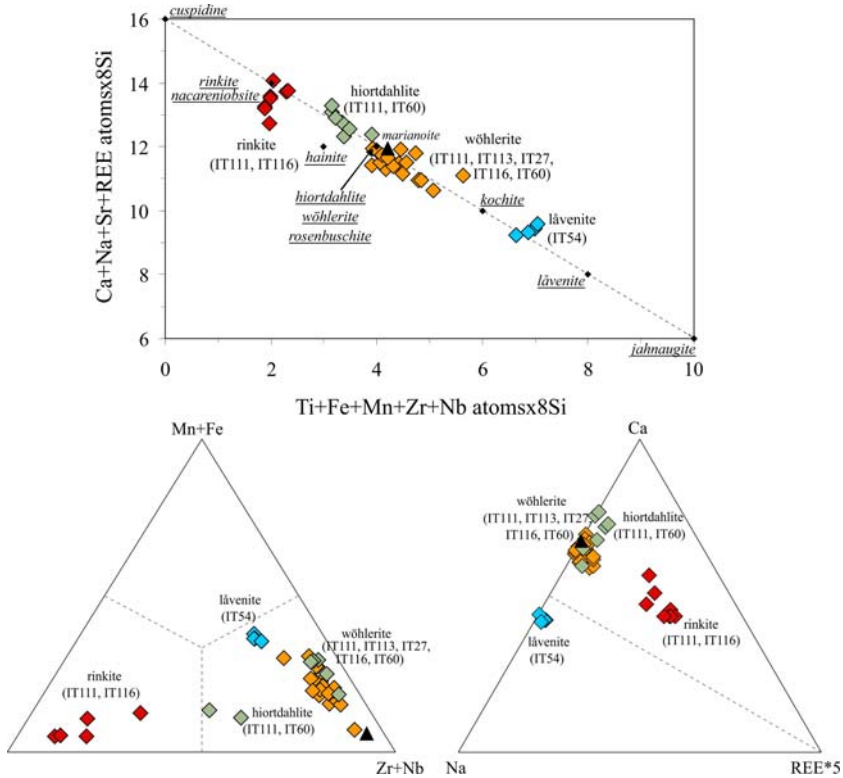

FIG. 8. Composition of the F-disilicates in the Itatiaia peralkaline nepheline syenites.

https://doi.org/10.1180/minmag.2016.080.122 Published online by Cambridge University Press

TABLE 5. Representative compositions of F-disilicates. Oxides and cations are listed based on site occupancy, according to their formula.

	A IT111	A IT111		A IT60	A IT111		A IT54	A IT54		A IT60	A IT111
(wt.%)	rinkite			hiortdahlite			låvenite			wöhlerite	
CaO	30.43	30.28		31.24	27.87		14.89	14.06		28.98	26.22
Na_2O	6.98	7.22		7.11	9.41		10.35	10.48		7.43	8.01
La_2O_3	5.21	6.17		0.37	0.31			0.06			0.56
Ce_2O_3	8.05	8.19		0.46				0.24		0.06	0.56
Nd_2O_3	0.65	1.16		0.30	0.59					0.10	0.39
Sm_2O_3					0.31		0.07	0.11		0.19	0.43
SrO	0.20	0.49		0.35						0.38	
TiO_2	8.49	7.84		0.95	6.98		6.10	5.75		1.30	1.97
FeO		0.25		0.82	0.50		4.75	4.78		0.62	0.48
MnO	0.45	0.23		2.07	1.50		6.16	5.96		2.08	2.42
MgO				0.08			0.43	0.41			
Y_2O_3		0.58									0.12
ZrO_2	0.84	1.81		17.76	16.78		20.82	22.89		14.08	14.67
Nb_2O_5	0.71	1.07		3.06	0.44		2.93	2.38		10.94	10.42
HfO_2											
ThO_2	0.37	0.14		0.23	0.02		0.34			0.10	0.19
UO_2				0.28			0.19				
SiO_2	30.08	29.76		30.53	31.35		30.88	30.37		30.38	30.43
Al_2O_3	0.14	0.19					0.26	0.13		0.22	0.17
F^-	6.89	7.33		6.33	7.43		5.43	5.02		3.62	3.80
Total 1	99.5	102.7		101.9	103.5		103.6	102.6		100.5	100.8
O = F	2.90	3.09		2.67	3.13		2.29	2.11		1.53	1.60
Total 2	96.6	99.6		99.3	100.4		101.3	100.5		99.0	99.2
Cations per 8 silicon atoms (apfu)											
Na	2	2							Na	3.76	4.06
Ca	2.42	2.26									
Na	1.58	1.74									
Sum	4.00	4.00	Ca	8.77	7.62	Ca	4.09	3.95	Ca	8.11	7.34
			Na	3.61	4.65	Na	5.15	5.33			
Ca	6.20	6.39	Sr	0.05	0.00				Sr	0.06	0.00
La	0.51	0.61	La	0.04	0.03	La	0.00	0.01	La	0.00	0.05
Ce	0.78	0.80	Ce	0.04	0.00	Ce	0.00	0.02	Ce	0.01	0.05
Nd	0.06	0.11	Nd	0.03	0.05	Nd	0.00	0.00	Nd	0.01	0.04
Sm	0.00	0.00	Sm	0.00	0.03	Sm	0.01	0.01	Sm	0.02	0.04
Sr	0.03	0.08	Sum	12.55	12.38	Sum	9.24	9.31	Sum	8.20	7.52
Sum	7.58	7.99									
Ti	1.69	1.57	Ti	0.19	1.34						
Fe	0.00	0.06	Fe	0.18	0.11	Fe	1.02	1.05	Ti	0.26	0.39
Mn	0.10	0.05	Mn	0.46	0.32	Mn	1.34	1.32	Fe	0.14	0.11
Mg	0.00	0.00	Mg	0.03	0.00	Mg	0.16	0.16	Zr	1.79	1.87
Zr	0.11	0.24	Zr	2.27	2.09	Sum	2.52	2.53	Nb	1.29	1.23
Nb	0.08	0.13	Nb	0.36	0.05				Mn	0.46	0.54
Y	0.00	0.08							Y	0.00	0.02
Hf	0.00	0.00	Hf	0.00	0.00	Zr	2.60	2.93	Th	0.01	0.01
Th	0.02	0.01	Th	0.01	0.00	Ti	1.18	1.13	Sum	3.94	4.15

(continued)

https://doi.org/10.1180/minmag.2016.080.122 Published online by Cambridge University Press

TABLE 5. (*contd*.)

	A IT111	A IT111		A IT60	A IT111		A IT54	A IT54		A IT60	A IT111
(wt.%)	rinkite			hiortdahlite			låvenite			wöhlerite	
U	0.00	0.00	U	0.02	0.00	Nb	0.34	0.28			
Sum	2.00	2.13	Sum	3.52	3.91	Sum	4.12	4.34			
Si	7.96	7.94	Si	8.00	8.00	Si	7.92	7.96	Si	7.93	7.95
Al	0.04	0.06	Al	0.00	0.00	Al	0.08	0.04	Al	0.07	0.05
Sum	8	8	Sum	8	8	Sum	8.00	8.00	Sum	8	8
O	28	28	O	28	28	O	28	28	O	28	28
F^-	4	4									
O^-	2.19	1.92	O^-, OH^-	2.77	2.16	O^-, OH^-	3.54	3.80	O^-, OH^-	4.89	4.73
F^-	1.81	2.08	F^-	5.23	5.84	F^-	4.46	4.20	F^-	3.11	3.27
Sum	4	4	Sum	8	8	Sum	8	8	Sum	8	8

A: nepheline-bearing rocks.

Apatite, britholite and monazite

Fluorapatite [$Ca_5(PO_4)_3F$] is the typical phosphate of the silica-oversaturated rocks where usually this is one of the early-crystallizing phases. In contrast, britholite [(Ca,*LREE*,Th)$_5$(SiO_4,PO_4)$_3$(OH,F)] commonly joins fluorapatite in the silica-undersaturated rocks (Fig. 9*a*,*b*,*c*). The composition of britholite has the highest SiO_2 (26.0 wt.%), $La_2O_3 + Ce_2O_3 + Nd_2O_3$ (66.4 wt.%) and the lowest P_2O_5 (0.3 wt.%), thus approaching the pure end-member, as typically observed worldwide (Melluso *et al.*, 2012*a*,*b*, 2014*b*; Vilalva *et al.*, 2013; Rønsbo, 2008; Macdonald *et al.*, 2013*b*). These phases are very low in Na, hence the typical and main cation substitution is $Ca^{2+} + P^{5+} \rightarrow LREE^{3+} + Si^{4+}$ (Fig. 9*b*). Thorium (up to 3.4 wt.% ThO_2) and U (up to 0.9 wt.% UO_2) show their highest concentrations in britholite (Table 6; Suppl. Table 9). Britholite has lower F (up to 4.7 wt.%) compared with apatite (F up to 7.9 wt.%), but both phases are poor in Cl (<0.07 wt.%), S (<0.65 wt.% SO_3) and Sr (SrO <2.2 wt.%).

Monazite [(Ce,La,Nd,Th)PO_4] was found in silica-oversaturated syenites and granites and in the corundum-bearing syenite (Fig. 3; Suppl. Table 9). The CaO and SiO_2 concentrations in this mineral are negligible (<1.41 wt.% CaO and SiO_2).

Fluorite

This mineral (CaF_2) is ubiquitous in both nepheline and quartz syenites of Itatiaia (Suppl. Table 9). No significant solid solutions have been noted.

Zircon

This mineral ($ZrSiO_4$) in quartz syenites sometimes has small blebs of exsolved thorite ($ThSiO_4$) and yttrialite [$(Y,Th)_2Si_2O_7$], a feature not commonly described elsewhere in igneous rocks (Fig. 3*c*–*i*), and is corroded in nepheline syenites to form later F-disilicates (Fig. 2; Suppl. Table 10).

Zirconolite

This mineral (ideally $CaZrTi_2O_7$) is observed in the nepheline syenites (ThO_2 up to 2 wt.% and negligible UO_2) and in silica-oversaturated rocks (ThO_2 up to 3.45 wt.%, UO_2 up to 2.33 wt.%), and is particularly abundant in the corundum-bearing syenite (ThO_2 up to 1.73 wt.%, UO_2 up to 1.22 wt.%) (Fig. 2; Suppl. Table 10). Zirconolite does not show any modal relationship with zircon, but possibly is an earlier phase in silica-oversaturated rocks. $\sum REE_2O_3$ concentrations reach values as high as 18.9 wt.%.

Baddeleyite

This mineral (ZrO_2) is far rarer than the other Zr-bearing phases (Suppl. Table 10); its limited stability is probably a function of the significant F in the system, stabilizing F-Zr disilicates such as låvenite, hiortdahlite and wöhlerite.

Pyrochlore

This mineral [ideally $(Na,Ca)_2Nb_2O_6(OH,F)$] is an ubiquitous phase and present in different varieties

https://doi.org/10.1180/minmag.2016.080.122 Published online by Cambridge University Press

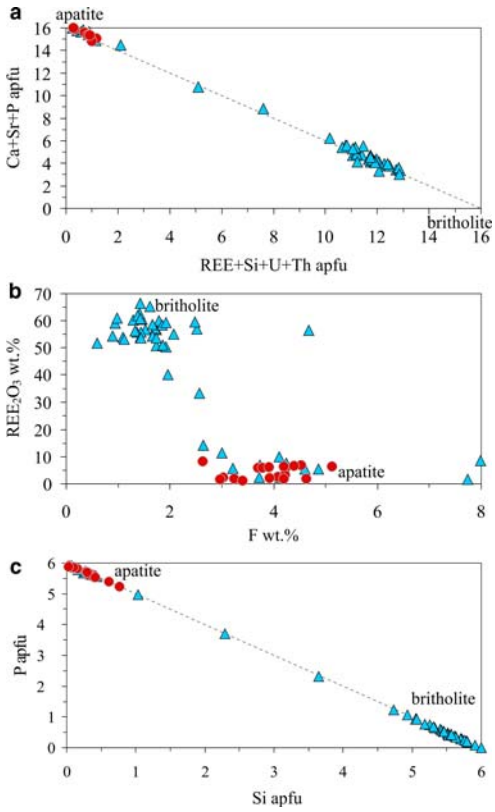

FIG. 9. (*a*,*b*,*c*) Apatite-britholite compositions of the Itatiaia rocks. Symbols: quartz-syenites and granites = red; nepheline syenites = blue; corundum-bearing syenites = green.

(Suppl. Table 10). In nepheline syenites it has variable concentrations in TiO_2 (4.2–12.3 wt.%), Na_2O (1.8–7.8 wt.%), $\sum REE_2O_3$ (3.4–10.7 wt.%) and F (1.6–6.9 wt.%) with low Y_2O_3 (0–2.3 wt.%). In corundum-bearing syenites the pyrochlore has highest concentrations in TiO_2 (17.6 wt.%) and $\sum REE_2O_3$ (27.5 wt.%) with low Na_2O (3.4 wt.%) and Y_2O_3 (1.6 wt.%) and negligible F.

In the granites pyrochlore, as an idiomorphic phase, is present as pyrochlore, plumbopyrochlore $[(Pb,Y,U,Ca)_{2-x}Nb_2O_6(OH)]$, uranopyrochlore $[(U,Ca,Ce)_2(Nb,Ta)_2O_6(OH,F)]$ and yttropyrochlore $[(Y,Na,Ca,U)_{1-2}(Nb,Ta,Ti)_2(O,OH)_7]$. Pyrochlore has variable concentrations of TiO_2 (0.6–10 wt.%), Na_2O (0.6–12.4 wt.%), $\sum REE_2O_3$ (2.5–11.4 wt.%), Y_2O_3 (0–6.4 wt.%) and F (0–5.1 wt.%). Plumbopyrochlore has 21.7–24.1 wt.% PbO, low TiO_2 (4.1–5.2 wt.%), Na_2O (1.2–2.6 wt.%), $\sum REE_2O_3$ (1.4–3 wt.%), Y_2O_3 (0.3–1.5 wt.%) and F (0.4–1.5 wt.%). Uranopyrochlore has high 33.8–34.8 wt.% UO_2, with low TiO_2 (1.5–1.9 wt.%), Na_2O (0.7–0.8 wt.%), $\sum REE_2O_3$ (2.1–4.6 wt.%), Y_2O_3 (0.7–1.4 wt.%) and F (0.2–0.3 wt.%). Yttropyrochlore has 16.8–18.8 wt.% Y_2O_3, 10.1–11 wt.% ThO_2 and 10.8–14.9 wt.% $\sum REE_2O_3$, with low TiO_2 (1.7–2 wt.%), Na_2O (0.2–0.3 wt.%) and F (1.2–1.3 wt.%).

Yttrocolumbite

This mineral [ideally $(Y,U,Fe^{2+})(Nb,Ta)O_4$] was found in nepheline syenite IT54 and granites IT102 (Suppl. Table 10). This phase is more rich in Th (up to 8 wt.% ThO_2) and U (up to 1.9 wt.% UO_2) in granite than in the nepheline syenite (up to 3.6 wt.% ThO_2 and up to 3.3 wt.% UO_2). Yttrocolumbite has also been found in other granites elsewhere (e.g. Cucciniello *et al.*, 2016).

Yttrialite

This mineral [ideally $(Y,Th)_2Si_2O_7$] is found in granite IT105, as an exsolution product of zircon (Fig. 3*c*–*i*).

Catapleiite

This phase (ideally $Na_2ZrSi_3O_9{\cdot}2H_2O$) is a secondary mineral in the peralkaline nepheline syenite IT60 (Fig. 2; Suppl. Table 10). The presence of this phase could mark the transition to hyperagpaitic (subsolidus?) compositions (Andersen *et al.*, 2010; Marks *et al.*, 2011).

Garnet

Garnet is a very rare phase at Itatiaia; it occurs in a few non-peralkaline nepheline syenites, and is always associated with Ca-amphibole. It is andradite-rich (66–88 mol.% andradite; TiO_2 = 1.2–4.6 wt.%; Al_2O_3 = 1.9–4.6 wt.%; Suppl. Table 11), and is almost identical in composition to the garnet of other intrusions in the area (e.g. at Morro de Sao João; Brotzu *et al.*, 2007).

Carbonates and fluorocarbonates

Secondary Fe-carbonates (mostly Mn-bearing siderite) are common in the interstices of the silica-oversaturated rocks, and rarely in the nepheline syenites (Suppl. Fig. 6; Suppl. Table 9). The same was observed for the bastnäsite-(Ce) [$(Ce,La)(CO_3)F$], a fluorocarbonate, found in quartz syenites (Fig. 3*b*) and, less frequently, in nepheline syenites.

Sulfides

Sphalerite (ZnS), pyrrhotite ($Fe_{0.95}S$) and galena (PbS) are usually tiny sulfide grains, ubiquitous in syenites and granites (Suppl. Table 12).

https://doi.org/10.1180/minmag.2016.080.122 Published online by Cambridge University Press

TABLE 6. Representative compositions of britholite. Oxides and cations are listed based on site occupancy, according to the formula.

	A IT113	A IT27	A IT111	A IT112	A IT24	A IT60	A IT116	A IT62
(wt.%)								
CaO	14.33	11.07	15.61	14.98	9.92	17.73	15.00	10.80
Na_2O	0.50	0.26	0.20	0.34	1.17		0.11	
SrO	1.14	1.07	0.85	0.74	0.79		0.49	
Y_2O_3	1.09	1.40		1.65	1.50		0.88	0.94
La_2O_3	22.19	21.31	22.95	14.91	25.20	18.93	18.04	28.42
Ce_2O_3	30.66	35.10	28.73	28.90	30.47	29.64	29.25	30.10
Nd_2O_3	3.94	5.43	3.41	7.19	3.02	5.25	6.52	2.45
Sm_2O_3				0.11		0.35		
Al_2O_3	0.15		0.17	0.39	1.22	0.18		
FeO				0.34	0.04			1.15
ThO_2	2.23	2.25	2.61	1.30	1.47	2.46	1.57	
UO_2		0.24				0.57		
SiO_2	20.58	20.38	19.19	19.86	22.46	18.18	19.52	26.04
P_2O_5	2.68	1.19	4.22	4.33	1.60	5.60	3.39	
SO_3		0.09		0.13	0.13	0.16	0.26	
F^-	1.73	1.37	2.07	1.86	1.66	1.43	1.09	0.98
Total 1	101.22	101.15	100.01	97.02	100.64	100.49	96.12	100.87
O = F, Cl	0.73	0.58	0.87	0.78	0.70	0.60	0.46	0.41
Total 2	100.49	100.58	99.14	96.23	99.94	99.89	95.66	100.46
REE_2O_3	56.79	61.83	55.09	51.00	58.69	53.83	53.82	60.96
Number of cations based on 16 cations per formula unit								
A site								
Ca	3.93	3.21	4.33	4.25	2.84	4.78	4.33	3.27
Na	0.25	0.13	0.10	0.18	0.61	0.00	0.06	0.00
Sr	0.17	0.17	0.13	0.11	0.12	0.00	0.08	0.00
Y	0.15	0.20	0.00	0.23	0.21	0.00	0.13	0.14
La	2.10	2.13	2.19	1.46	2.48	1.76	1.79	2.96
Ce	2.87	3.48	2.72	2.80	2.98	2.73	2.89	3.11
Nd	0.36	0.52	0.32	0.68	0.29	0.47	0.63	0.25
Sm	0.00	0.00	0.00	0.01	0.00	0.03	0.00	0.00
Al	0.05	0.00	0.05	0.12	0.38	0.05	0.00	0.00
Fe	0.00	0.00	0.00	0.08	0.01	0.00	0.00	0.27
Th	0.13	0.14	0.15	0.08	0.09	0.14	0.10	0.00
U	0.00	0.01	0.00	0.00	0.00	0.03	0.00	0.00
Sum	10	10	10	10	10	10	10	10
T site								
Si	5.40	5.70	5.06	5.04	5.64	4.73	5.18	6.00
P	0.60	0.28	0.94	0.93	0.34	1.24	0.76	0.00
S	0.00	0.02	0.00	0.02	0.02	0.03	0.05	0.00
Sum	6	6	6	6	6	6	6	6
F^-	1.39	1.17	1.65	1.49	1.33	1.14	0.92	0.79
OH^-	0.61	0.83	0.35	0.51	0.67	0.67	1.08	1.21
Sum	2	2	2	2	2	2	2	2

A: nepheline-bearing rocks.

https://doi.org/10.1180/minmag.2016.080.122 Published online by Cambridge University Press

A number of other μm-sized phases have been proved difficult to identify with just compositional data and optical observations (Suppl. Table 10).

Geochemistry

The main geochemical variations of the Itatiaia rocks have already been described in Brotzu *et al.* (1997), hence only new data are highlighted here. The rocks have a very evolved composition (MgO = 0.01 to 1.7 wt.%). The SiO_2 concentration of nepheline syenites and corundum-bearing syenites range from 55 to 63.2 wt.% (average 58.6 wt.%), showing only limited overlap with the silica-oversaturated rocks (SiO_2 from 61.4 to 73.2 wt.%; average 65.9 wt.%). The nepheline syenites and the corundum-bearing syenites can also be distinguished from the silica-oversaturated rocks for their higher Al_2O_3 (18.3–24.7 wt.%, average 21.2 wt.% *vs*. 14.4–20.1 wt.%, average 17.9 wt.%), K_2O (5.7–11.4 wt.%, average 7.7 wt.% *vs*. 4.3–8.6 wt.%, average 5.9 wt.%), $Na_2O + K_2O$ (11.7–18.7 wt.%, average 15.0 wt.% *vs*. 8.2–12.9 wt.%, average 11.3 wt.%, respectively). Clear correlation trends of major elements *vs*. SiO_2 are visible for TiO_2, Al_2O_3, MgO and K_2O for the silica-oversaturated rocks. In contrast, the major-element variation of the alkali-rich syenites with SiO_2 is less clear. The trace-element concentrations spread over a wide range (Table 1; Suppl. Fig. 7). The Cr, Ni and Sc contents are close to or below the detection limits. Vanadium ranges from 14 to 39 ppm, Ga varies similarly (19–50 ppm) and Zn ranges from 80 to 300 ppm. Strontium varies from 40 to 2317 ppm in the nepheline syenites and from 16 to 1423 ppm in the silica-oversaturated rocks; the Ba concentration varies from negligible to 657 ppm in the nepheline syenites and from 11 to 1225 ppm in the silica-oversaturated rocks; the Rb concentration varies from 115 to 251 ppm in the nepheline syenites and from 142 to 372 ppm in the silica-oversaturated rocks. Yttrium, Zr, Nb, Th and U also have a very wide range of compositions (Table 2). The $\sum REE$ concentrations vary from 467 to 1246 ppm in the nepheline syenites and from 412 to 720 ppm in the silica-oversaturated rocks. The chondrite-normalized *REE* distribution patterns of the nepheline syenites are highly fractionated (La_n/Yb_n from 32 to 69; the subscript 'n' means chondrite-normalized values), and have a concave upwards pattern in the least Mg-rich samples (Gd_n/Yb_n from 0.4 to 3.7) and Eu peaks or troughs (Eu/Eu* from 0.72 to 1.3; Fig. 10*a*; Table 1). The corundum-bearing syenite IT42 has a small Eu trough (Eu/Eu* = 0.79), and highly fractionated pattern ($La_n/Yb_n = 69$; La = 316 ppm, $La_n = 1016$). Quartz syenites have lower La_n/Yb_n (11–33), and, with one exception, variable but strong Eu troughs (Eu/Eu* = 0.09–0.92), which are explained broadly by subtraction of Eu^{2+}-rich alkali feldspar. Sample IT66, the most MgO-rich quartz syenite, has no Eu trough (Fig. 10*b*). The *REE* patterns of the Itatiaia rocks normalized to the concentration of sample IT66 are shown in Fig. 10*c*, *d*. The increasing degree of evolution is accompanied by different *REE* patterns: the least MgO-rich nepheline syenites have the lowest concentration of middle *REE* (*MREE*); the most MgO-poor quartz syenites and the granites are characterized by an enrichment in heavy rare-earth elements (*HREE*), less so in *LREE*, highlighting a marked Eu trough that is nearly absent (or even present as a peak) in the nepheline syenites. It is straightforward to link this quite contrasting geochemical behaviour of *REE* to the effects of different scavenging *REE*-bearing phases acting in different magmas during their crystallization. The primitive mantle-normalized distribution patterns of the Itatiaia rocks are reported in Suppl. Fig. 8 and show the expected (increasing) troughs at Ba, Sr, Eu, P and Ti typical of evolved rocks, which are caused by extensive removal of one or two feldspars, Fe-Ti oxides and apatite from more mafic magmas (e.g. Brotzu *et al.*, 1997). The mafic dykes of the Serra do Mar province, some crosscutting the metamorphic septum between Itatiaia and Passa Quatro, range in composition from alkali basalt, through basanite and tephrite, to foidite (Brotzu *et al.*, 2005 and references therein). They are highly enriched in the most incompatible elements, and have smooth primitive mantle-normalized patterns peaking at Ba (100–450 × PM; PM = primitive mantle) and Nb (60–250 × PM; primitive mantle values of Lyubetskaya and Korenaga, 2007; Suppl. Fig. 8). The chondrite-normalized *REE* patterns are steep ($La_n/Yb_n = 14$–30) and lack Eu troughs. Dykes with evolved composition (trachybasalts, trachyandesites, phonotephrites, trachytes, phonolites) are also found throughout the Serra do Mar, and represent the parental magmas of the intrusions (Brotzu *et al.*, 2005; 2007; Enrich *et al.*, 2005; Azzone *et al.*, 2009; Menezes *et al.*, 2015).

Discussion

Significance of accessory phases in strongly evolved melts

The Itatiaia massif is an important place to study petrogenetic processes in the residual fractions of

https://doi.org/10.1180/minmag.2016.080.122 Published online by Cambridge University Press

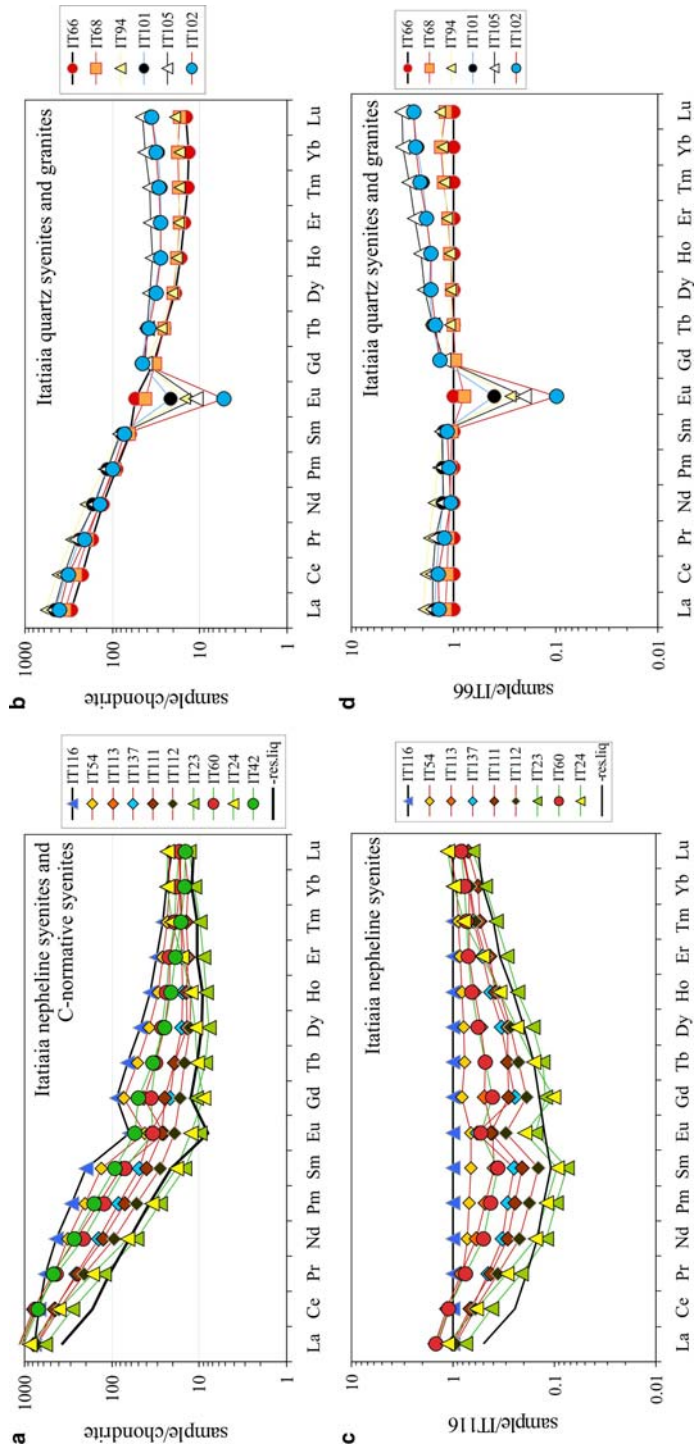

FIG. 10. (*a*) and (*b*) *REE* patterns of the Itatiaia bulk-rocks. Normalization values of Boynton (1984). The black thick pattern is the result of 3% removal of titanite from the nepheline syenite IT116. (*c*) and (*d*) *REE* patterns after normalization for the least evolved syenites of each compositional group. The partition coefficients of titanite are taken from Olin and Wolff (2012). Prometium is interpolated.

https://doi.org/10.1180/minmag.2016.080.122 Published online by Cambridge University Press

liquid during and after alkali feldspar crystallization in low-pressure, slowly cooled, trachytic/phonolitic intrusions of potassic affinity. The Itatiaia magmatic reservoir was filled by multiple intrusions of hydrous, F-rich, Cl- and SO_3-poor, evolved phonolitic-trachytic-rhyolitic magmas, which have their own compositional trends, and that cannot be considered strictly as co-magmatic batches.

The typical assemblage of the nepheline syenites is alkali feldspar and nepheline, the latter first interstitial and then idiomorphic, together with minor clinopyroxene, oxides, titanite, amphibole, biotite and apatite. The F-disilicates, britholite and pyrophanite are the distinguishing accessories of the peralkaline nepheline syenites. The corundum-bearing syenite has zircon, zirconolite, Mn-rich ilmenite and monazite as the main accessory phases, lacks clinopyroxene and amphibole, and has Al-rich mica and hercynite (and the corundum grains themselves). This rock has no trace of resorbed phases, indicating that, if major crustal contamination by Al-rich contaminants (such as metapelites) did take place, it occurred well before liquidus temperature was approached. Other corundum-normative syenites are chemically indistinguishable from normal alkali-rich nepheline syenites. The typical assemblage of quartz syenites and granites is: alkali feldspar, quartz, opaque oxides and amphibole, with lower amounts of plagioclase, biotite, clinopyroxene and apatite. Chevkinite/perrierite is the main accessory phase of this group.

The presence of chevkinite/perrierite (±allanite) and the abundance of pseudobrookite in the quartz syenites, and the Ca-F-disilicates, britholite and pyrophanite-rich compositions in the nepheline syenites are among the most striking differences in the accessory phase assemblages (Table 2). Note that, whilst rinkite, wöhlerite, hiortdahlite and låvenite are known only as late-stage phases in silica-undersaturated rocks, chevkinite is known to occur in both silica-undersaturated (though exceedingly rare, and possibly overlooked) and silica-oversaturated igneous rocks (Cellai *et al.*, 1993; Macdonald and Belkin, 2002; Troll *et al.*, 2003; Carlier and Lorand, 2008; Melluso *et al.*, 2014*a*), although this is not the case in the Itatiaia rocks. The cause of these two differing assemblages cannot be related unambiguously to differing silica activity, fluorine fugacity or *REE* concentrations. There is no clear correlation between the degree of magmatic evolution, as represented by MgO concentration or other differentiation indices, and the accessory phase assemblages of the syenites and granites (Table 2). Regardless, the influence of melt polymerization and volatile concentrations, taking into account that fluorine is ubiquitous in both silica-undersaturated and silica-oversaturated rocks (Figs 2, 3 and Table 2) make the phase assemblages intriguing and worthy of further discussion.

The transition from metaluminous (i.e. miaskitic) to peralkaline conditions in the nepheline syenites is accompanied by two main mineral reactions visible in thin section: (1) titanite is corroded and becomes smaller; (2) zircon + fluorite are unstable and react to form F-disilicates (actually mantling both phases; Fig. 2*e–j*). The stabilization of F-disilicates, which are also found without zircon and fluorite cores, is possibly in response to a decreasing availability of fluorine, and locally increasing Ca and Na after the extensive crystallization of K-rich alkali feldspar. The transition to peralkaline conditions in the quartz-syenites and granites is subtle. Actually, true peralkaline granites are not found at Itatiaia, being all silica-oversaturated rocks characterized by P.I. <1 (Suppl. Fig. 1).

The F-disilicates of Itatiaia are commonly found in other syenites and peralkaline silica-undersaturated rocks worldwide (e.g. Woolley and Platt, 1986, 1988; Moreau *et al.*, 1996; Atencio *et al.*, 1999; Carbonin *et al.*, 2005; Ridolfi *et al.*, 2006; Andersen *et al.*, 2010, 2013; Lustrino *et al.*, 2012; Melluso *et al.*, 2012*a*; 2014*b*; Rønsbo *et al.*, 2014). They are the result of the concentration of the remaining fluorine (after fluorite crystallization and/or fluorite resorption) and other elements in the interstitial liquids after the dominant crystallization of felsic phases, but the (apparently random) combination of different disilicates in a given rock, their widely changing Ca/Na, Mn/Fe, Ti/Zr and Zr/Nb ratios, and the concentration of *REE* are still poorly understood from a thermodynamic point of view (Andersen *et al.*, 2010). The variable element concentrations of these phases are very difficult to explain without invoking a 'local' concentration of elements, including F and H_2O. This is also particularly evident when considering that other locally crystallized (or co-crystallized) phases, such as pyrochlore, britholite, yttrocolumbite, yttrialite, zircon, zirconolite, bastnäsite, Fe-Ti oxides and fluorite can be found in the same thin section.

Origin of the variable silica saturation in the Itatiaia rocks

Brotzu *et al.* (1997) reported a variation in initial $^{87}Sr/^{86}Sr$ from 0.70491 to 0.70542 in the nepheline syenites and from 0.70621 to 0.70663 in the silica-

https://doi.org/10.1180/minmag.2016.080.122 Published online by Cambridge University Press

oversaturated rocks, with the corundum-bearing syenite plotting in the nepheline syenite range ($^{87}Sr/^{86}Sr = 0.70537$). The $^{87}Sr/^{86}Sr$ of the nepheline syenites is well within the range of the associated mafic magmas (0.7037–0.7055 for igneous rocks with MgO >5 wt.%; Brotzu *et al.*, 2005, 2007 and references therein). The slightly higher $^{87}Sr/^{86}Sr$ of the silica-oversaturated samples, coupled with higher SiO_2, is an indication of crustal contamination, a typical feature of quartz-bearing syenitic rocks found in the same intrusions as nepheline-bearing varieties (e.g. Foland *et al.*, 1993). Indeed, a moderate amount of bulk mixing (18–20%) between Sr-rich nepheline syenites and the most radiogenic basement rocks of the area (Tupinambá *et al.*, 2012) may account for the higher $^{87}Sr/^{86}Sr$ of the quartz syenites.

The Itatiaia rocks cannot be considered as strictly comagmatic, the composition of intrusive samples being a result of feldspar accumulation (responsible for Eu peaks in chondrite-normalized *REE* patterns) or local variations not related to the degree of magmatic evolution (such as redistribution of phases or slightly different liquid lines of descent; Brotzu *et al.*, 1997, 2005).

Modelling magmatic evolution and the role of titanite removal

Representative mass-balance calculations (reported in Table 7) indicate that the transition to the most evolved nepheline syenites (e.g. samples IT113 to IT23), assumed to be representative of liquid compositions, can be obtained after removal of ~30% of the syenitic assemblages from the least evolved nepheline syenite. With the same assumption, the transition from quartz syenites to granites (e.g. sample IT66 to IT105) is obtained through ~64% removal of a syenitic assemblage (Table 7). In both examples, removal of felsic minerals is dominant, as expected from the petrographic features of the samples. The role of phases such as titanite, oxides and mafic phases in controlling major-element variations cannot be constrained precisely (Suppl. Fig. 7). Removal of very small amounts of titanite from the nepheline syenite IT116 almost perfectly matches the *REE* composition of the most evolved nepheline syenites (Fig. 10*a*,*c*). In contrast, significant removal of amphibole in the quartz-syenites can cause less-concave patterns and still-evident Eu troughs (Fig. 10*b*,*d*). The role of apatite may be roughly similar to that of titanite in the fractionation of *MREE*, and these two phases commonly co-crystallize in trachytic (*s.l.*) magmas, but typical magmatic apatite has significantly lower partition coefficients (by a factor of 2–3) than typical magmatic titanite (e.g. Olin and Wolff, 2012; Fedele *et al.*, 2015). The late appearance of britholite (found as rims around apatite or discrete crystals in the peralkaline syenites) indicates its very limited role to modify already evolved compositions. The relatively high *LREE* concentration in britholite can be achieved in the absence of major *REE* subtraction of earlier-formed apatite. Nevertheless, the latest, F-H_2O-rich fraction of magmas in both silica-oversaturated and silica-undersaturated syenites confirm the late concentration of *REE* and HFSE-rich phases after or during feldspar (±nepheline, ±quartz) crystallization. Given the interstitial position of the phases hosting rare-metal elements, it is difficult to demonstrate their removal during late magmatic evolution, but the removal of early titanite and alkali feldspar in the Itatiaia syenites is important, and provides a limit to the *REE* enrichment in more residual liquids, making the *MREE* compatible, with *LREE* and *HREE* having variably compatible behaviour (e.g. Lustrino *et al.*, 2012). Moreover, this is further evidence that many elements usually defined as 'strongly incompatible' in evolved tholeiitic, calcalkaline or silicic peralkaline magmas (pantellerites, comendites and 'alkali granites') are not so in trachytic/phonolitic magmatic systems (e.g. Ronga *et al.*, 2010; Guarino *et al.*, 2011; Melluso *et al.*, 2010, 2014*a*; Fedele *et al.*, 2015; Mbouwou *et al.*, 2015).

Oxygen fugacity, silica activity and chemical variations of the mafic phases; causes of titanite stability, Fe-Mn partitioning

Major attempts have been made to qualitatively model the links between mineral assemblages of peralkaline rocks with oxide activity or oxygen fugacity (e.g. Andersen *et al.*, 2010; Marks *et al.*, 2011). The works of Andersen *et al.* (2010) and Borst *et al.* (2016) are addressed to a more Cl-rich environment than that observed in this present study, given the systematic presence of eudialyte (mineral assemblages not matching those of this present study) and to more extreme crystallization conditions, grading to the post-magmatic/ hydrothermal. Eudialyte was not found in the Itatiaia peralkaline rocks to date: however, it was found in phonolite dykes of the nearby Passa Quatro complex (Brotzu *et al.*, 1992) and in other complexes of the area (e.g. Monte de Trigo island; Enrich *et al.*, 2009; Poços de

https://doi.org/10.1180/minmag.2016.080.122 Published online by Cambridge University Press

TABLE 7. Major-element mass-balance calculations and a fractional crystallization model involving titanite removal from the least evolved nepheline syenite. The partition coefficients are those of Olin and Wolff (2012) or interpolated (italics).

From	A IT112	A IT112	A IT113	A IT113	A IT113	Q IT66	Q IT66	Q IT66	Q IT66	Q IT68	Q IT68	Q IT68
to	A IT23	A IT23	A IT23	A IT23	A IT24	Q IT102	Q IT105	Q IT105	Q IT105	Q IT105	Q IT102	Q IT102
Alkali feldspar	–8.55	–20.2	–25.8	–13.8	–17.1	–31.2	–35.1	–32.7	–27.6	–27.7	–30.9	–27.0
Plagioclase		–5.04	–5.53	–11.5	–13.4	–25.4	–20.6	–20.2	–19.4	–13.4	–20.6	–20.5
Nepheline	–4.84	–4.57	–8.14	–2.19	–3.87							
Titanite	–0.58	–1.15	–1.03	–0.92	–0.89							
Clinopyroxene	–1.93	–1.34	–2.39	–1.03	–0.13				–1.10			
Amphibole						–1.92	–4.84	–3.62		–3.98	–4.30	–2.27
Magnetite	–0.14					–1.60	–1.19	–1.20	–1.44	–0.35	–0.77	–0.84
Ilmente						–0.87	–1.24	–0.99		–0.92	–1.21	–0.83
Biotite						–3.65		–1.46	–5.02			–2.41
Apatite						–0.69	–0.51	–0.64	–0.84	–0.32	–0.12	–0.32
Sub. Sol. (%)	–16.0	–32.3	–42.9	–29.4	–35.4	–65.4	–63.5	–60.8	–55.4	–46.7	–57.9	–54.2
f (%)	84.0	67.7	57.1	70.6	64.6	34.6	36.5	39.2	44.6	53.3	42.1	45.8
ΣR^2	0.21	0.48	0.41	0.30	0.36	0.12	0.16	0.15	0.20	0.10	0.27	0.24

Titanite fractional crystallization model

	Chondrite normalized			IT116-0.01 ttn	IT116-0.02 ttn	IT116-0.03 ttn
	IT116	IT116	Kd titanite	f = 99%	f = 98%	f = 97%
La (ppm)	237.0	765	24	607	480	379
Ce	549.0	679	47	428	268	167
Pr	69.9	573	56	330	189	107
Nd	260.0	433	64	230	121	64
Pm		*291*	*69*	*147*	*74*	*37*
Sm	38.2	196	74	94	45	21
Eu	4.7	64	69	32	16	8
Gd	22.7	88	65	46	24	12
Tb	3.1	65	61	36	19	11
Dy	15.2	47	54	28	16	9

(continued)

TABLE 7. (*contd.*)

From	A IT112	A IT112	A IT113	A IT113	A IT113	Q IT66	Q IT66	Q IT66	Q IT68	Q IT68	Q IT68
to	A IT23	A IT23	A IT23	A IT23	A IT24	Q IT102	Q IT105	Q IT105	Q IT105	Q IT102	Q IT102
Ho	2.6		36		46			23	15		9
Er	6.5		31		36			22	15		11
Tm	0.9		26		31			19	14		11
Yb	5.0		24		23			19	15		12
Lu	0.7		21		20			17	14		12

ΣR^2 = sum of the squared residuals.
f = fraction of remaining liquid.
A: nepheline-bearing rocks; Q: quartz-bearing rocks.

Caldas), suggesting its limited role in the petrogenesis of the Brazilian syenites, overall.

Marks *et al.* (2011) show that the presence of arfvedsonite rather than aegirine is to be linked to a relatively lower fO_2. The stoichiometry of amphibole of the quartz syenites indeed indicate a significant presence of Fe^{2+} (Suppl. Fig. 3), but we also observe that the magnetite-ilmenite pairs of quartz syenites and granites, the rocks with the highest amount of sodic amphibole, give a range of equilibration temperatures and oxygen fugacities well above the NiNiO buffer, trending towards the magnetite-haematite (MH) buffer, thus indicating a highly oxidized environment (Fig. 6*c*). Moreover, it should be noted that the presence of Fe^{3+}-rich clinopyroxene is better related to the onset of peralkaline conditions, than to increased oxygen fugacity in the magmas. The total lack of aenigmatite and fayalite at Itatiaia hampers attempts to better constrain the oxygen fugacity of the system, also using modified versions of the *QUILF* code (Andersen *et al.*, 1993). A relatively high oxygen fugacity (higher than the QFM buffer) is required for the stability of titanite at magmatic temperatures, in the presence of quartz, though variables other than oxygen fugacity or silica activity are also important for titanite formation (e.g. Xirouchakis and Lindsley, 1998; Ryabchikov and Kogarko, 2006; Melluso *et al.*, 2012*b*).

The variation of Mn in the clinopyroxene has been also observed in other alkaline suites (e.g. Lustrino *et al.*, 2012; Melluso *et al.*, 2014*b*), and can be interpreted as an effect of co-crystallization with several other Mn-rich phases (ilmenite-pyrophanite, F-disilicates and so on) and to the difficulty of an Fe^{2+}-Mn substitution in a pyroxene that is poor in divalent cations (Suppl. Fig. 2). If peralkaline conditions are attained, Mn avoids Na-clinopyroxene and enters other accessory phases. In this respect, the diagram FeO_t–MnO (Fig. 11) shows many interesting aspects of the petrogenesis of evolved igneous rocks, i.e. those where MgO (and Fe as well) is present in low concentrations, and the main cationic substitution in the mafic phases is thus Fe → Mn. When compared to the limited range of FeO_t/MnO in the bulk-rock compositions, there is a range of five orders of magnitude of this ratio in the mafic phases (from ~0.01 to ~1500), with the lowest ratios found in F-disilicates, pyrochlore and ilmenite and, to a lesser extent, biotite (i.e. Fe^{2+}-dominated phases), and the highest in magnetite, aegirine and pseudobrookite (i.e. the Fe^{3+}-rich phases). Titanite is an accessory phase that has roughly the

https://doi.org/10.1180/minmag.2016.080.122 Published online by Cambridge University Press

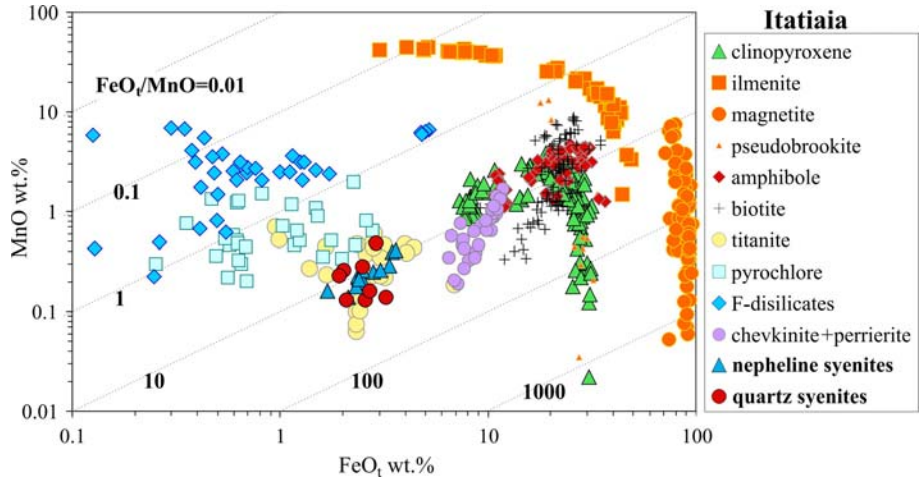

FIG. 11. FeO_t–MnO (wt.%) diagram with the composition of mafic phases of Itatiaia and the host rocks. Note the logarithmic scales and the different FeO/MnO ratios.

same concentration of FeO_t and MnO as the bulk-rocks. It is evident that this range of variations of FeO_t/MnO in coexisting phases depends upon their structure, isomorphic substitutions and co-crystallization with other competing phases. In general, Mn cannot be neglected in the phase stability of trachytic/phonolitic systems, as it may induce stability of accessory phases instead of others. This complex Fe-Mn partitioning of naturally occurring minerals could provide significant interest for detailed geothermobarometric studies (e.g. Andersen *et al.*, 2010; Melluso *et al.*, 2010, 2012*a*; Marks *et al.*, 2011; Giehl *et al.*, 2013).

Conclusions

The crystallization of feldspar, nepheline or quartz, Fe-Ti oxides, amphibole, clinopyroxene, titanite and apatite in the Itatiaia syenitic rocks led to the formation of low-Mg, low-Fe magmatic liquids plotting close to, or at, the minimum melt compositions in pertinent phase diagrams, and to the crystallization of a plethora of interstitial phases very rich in *REE* and HFSE. Many of these near-solidus minerals are related to the degree of silica saturation of the environment, such as the assemblage F-disilicates + pyrophanite + britholite in the nepheline syenites (+ aegirine + nepheline + alkali feldspar) *vs*. the assemblage chevkinite/perrierite + zircon + monazite in the quartz syenites and granites (+ alkali feldspar + Fe-Ti oxides + alkali amphibole + quartz). Further, the composition and compositional evolution of the major mafic phases (biotite, amphibole, clinopyroxene, oxides) indicates different physico-chemical conditions between quartz-bearing and nepheline-bearing samples. Such evident variation of the composition of major and accessory phases can also be used as a lithological marker. The bulk-rock evolution is generally consistent with the 'non hyperagpaitic' mineral assemblages, and with the ultimate derivation of the Itatiaia rocks through extensive fractional crystallization of volatile-rich (mainly H_2O and F) basanitic to alkali basaltic mafic parental magmas, that may have been accompanied by limited crustal contamination (for the genesis of the quartz-bearing syenites). It is noteworthy that eventual open-system processes took place at supraliquidus conditions, given that there is no trace of resorbed xenocrysts. The actual reliability of calculating the oxygen fugacity of highly evolved magmas by using coexisting mineral compositions requires further study.

Acknowledgements

Pietro Brotzu, Celso Gomes, Lucio Morbidelli and Excelso Ruberti are a neverending source of scientific advice and guide into various aspects of alkaline magmatism in Brazil and elsewhere. Ray Macdonald, Tom Andersen, Michael Marks, Silvio Vlach and John White are thanked for interesting discussions on phase equilibria and mineralogy of peralkaline rocks over the years; Dr. Piotr Dzierzanowski (Faculty of Geology, University of Warsaw) kindly analysed perrierite and

https://doi.org/10.1180/minmag.2016.080.122 Published online by Cambridge University Press

allanite crystals of sample IT66. Sergio Bravi prepared polished thin sections and Ciro Cucciniello performed the new XRF analyses. Raul Carampin is thanked for his help during work at the Padua microprobe in the late 90 s. The comments of two anonymous reviewers, the Associate Editor Jason Harvey and Roger Mitchell helped to improve an early version of this manuscript. This research benefited from grants from PRIN 2010-2011 (20107ESMX9_001) and Fondi Ricerca Dipartimentale to L. Melluso.

References

Andersen, D.J., Lindsley, D.H. and Davidson, P.M. (1993) QUILF: a Pascal program to assess equilibria among Fe-Mn-Mg-Ti oxides, pyroxenes, olivine and quartz. *Computers and Geosciences*, **19**, 1333–1350.

Andersen, T., Erambert, M., Larsen, A.O. and Selbekk, R. S. (2010) Petrology of nepheline syenite pegmatites in the Oslo Rift, Norway: zirconium silicate mineral assemblages as indicators of alkalinity and volatile fugacity in mildly agpaitic magmas. *Journal of Petrology*, **51**, 2303–2325.

Andersen, T., Erambert, M., Larsen, A.O. and Selbekk, R. S. (2013) Petrology of nepheline syenite pegmatites in the Oslo Rift, Norway: Zr and Ti mineral assemblages in miaskitic and agpaitic pegmatites in the Larvik Plutonic complex. *Mineralogia*, **44**, 61–98.

Atencio, D., Coutinho, J.M.V., Ulbrich, M.N.C., Vlach, S. R.F., Rastvetaeva, R.K. and Pushcharovky, D.Yu. (1999) Hainite from Pocos de Caldas, Minas Gerais, Brazil. *The Canadian Mineralogist*, **37**, 91–98.

Azzone, R.A., Ruberti, E., Enrich, G.E.R. and Gomes, C. B. (2009) Zr- and Ba-rich minerals from the Ponte Nova alkaline mafic-ultramafic massif, southeastern Brazil: indication of an enriched mantle source. *The Canadian Mineralogist*, **47**, 1087–1103.

Baginski, B. and Macdonald, R. (2013) The chevkinite group: underestimated accessory phases from a wide range of parageneses. *Mineralogia*, **44**, https://doi.org/10.2478/mipo-2013-0006.

Barbieri, M., Beccaluva, L., Brotzu, P., Conte, A., Garbarino, C., Gomes, C.B., Loss, E.L., Macciotta, G., Morbidelli, L., Scheibe, L.F., Tamura, R.M. and Traversa, G. (1987) Petrological and geochemical studies of alkaline rocks from continental Brazil. 1. The phonolite suite from Piratini, R.S. *Geochimica Brasiliensis*, **1**, 109–138.

Bellieni, G., Montes-Lauar, C.R., De Min, A., Piccirillo, E.M., Cavazzini, G., Melfi, A.J. and Pacca, I.G. (1990) Early and Late Cretaceous magmatism from São Sebastião Island (SE Brazil): geochemistry and petrology. *Geochimica Brasiliensis*, **4**, 59–83.

Bennio, L., Brotzu, P., Gomes, C.B., D'Antonio, M., Lustrino, M., Melluso, L., Morbidelli, L. and Ruberti, E. (2002) Petrological, geochemical and Sr-Nd isotopic features of alkaline rocks from the Arraial do Cabo Frio peninsula (southeastern Brazil). *Periodico di Mineralogia*, **71**, 137–158.

Bennio, L., Brotzu, P., D'Antonio, M., Feraud, G., Gomes, C.B., Marzoli, A., Melluso, L., Morbidelli, L., Morra, V., Rapaille, C. and Ruberti, E. (2003) The tholeiitic dyke swarm of the Arraial do Cabo peninsula (SE Brazil): $^{39}Ar/^{40}Ar$ ages, petrogenesis and regional significance. *Journal of South American Earth Sciences*, **16**, 163–176.

Borst, A.M., Friis, H., Andersen, T., Nielsen, T.F.D., Waight, T.E. and Smit, M.A. (2016) Zirconosilicates in the kakortokites of the Ilímaussaq complex, South Greenland: Implications for fluid evolution and high-field-strength and rare-earth element mineralization in agpaitic systems. *Mineralogical Magazine*, **80**, 5–30.

Bowles, J.F.W. (1988) Definition and range of composition of naturally occurring minerals with the pseudobrookite structure. *American Mineralogist*, **73**, 1377–1383.

Boynton, W.B. (1984) Cosmochemistry of Rare Earth Elements: meteorite studies. Pp. 63–114 in: *Rare Earth Element Geochemistry* (P. Henderson, editor). Elsevier, Amsterdam.

Brotzu, P., Beccaluva, L., Conte, A., Fonseca, M., Garbarino, C., Gomes, C.B., Leong, R., Macciotta, G., Mansur, R.L., Melluso, L., Morbidelli, L., Ruberti, E., Sigolo, J.B., Traversa, G. and Valença, J.G. (1989) Petrological and geochemical studies of alkaline rocks from continental Brazil. 8. The syenitic intrusion of Morro Redondo, R.J. *Geochimica Brasiliensis*, **3**, 63–80.

Brotzu, P., Barbieri, M., Beccaluva, L., Garbarino, C., Gomes, C.B., Macciotta, G., Melluso, L., Morbidelli, L., Ruberti, E., Sigolo, J.B. and Traversa, G. (1992) Petrology and geochemistry of the Passa Quatro alkaline complex, southeastern Brazil. *Journal of South American Earth Sciences*, **6**, 237–252.

Brotzu, P., Gomes, C.B., Melluso, L., Morbidelli, L., Morra, V. and Ruberti, E. (1997) Petrogenesis of coexisting SiO_2-undersaturated to SiO_2-oversaturated felsic igneous rocks: the alkaline complex of Itatiaia, southeastern Brazil. *Lithos*, **40**, 133–156.

Brotzu, P., Melluso, L., d'Amelio, F. and Lustrino, M. (2005) Mafic/ultramafic dykes and felsic intrusions with potassic to ultrapotassic affinity in the Serra do Mar province: a review. Pp. 443–472 in: *Mesozoic to Cenozoic Alkaline Magmatism in the Brazilian Platform* (P. Comin-Chiaramonti and C.B. Gomes, editors). FAPESP, São Paulo, Brazil.

Brotzu, P., Melluso, L., Bennio, L., Gomes, C.B., Lustrino, M., Morbidelli, L., Morra, V., Ruberti, E., Tassinari, C. C.G. and D'Antonio, M. (2007) Petrogenesis of the Cenozoic potassic alkaline complex of Morro de São

https://doi.org/10.1180/minmag.2016.080.122 Published online by Cambridge University Press

João, southeastern Brazil. *Journal of South American Earth Sciences*, **24**, 93–115.

Carbonin, S., Liziero, F. and Fuso, C. (2005) Mineral chemistry of accessory minerals in alkaline complexes from the Alto Paraguay Province. Pp. 149–158 in: *Mesozoic to Cenozoic Alkaline Magmatism in the Brazilian Platform* (P. Comin-Chiaramonti and C.B. Gomes, editors). FAPESP, São Paulo, Brazil.

Carlier, G. and Lorand, J.-P. (2008) Zr-rich accessory minerals (titanite, perrierite, zirconolite, baddeleyite) record strong oxidation associated with magma mixing in the south Peruvian potassic province. *Lithos*, **104**, 54–70.

Cellai, D., Conticelli, S. and Diella, V. (1993) Perrierite-chevkinite in igneous ultrapotassic rocks from Central Italy: chemical data and their petrological significance. *Periodico di Mineralogia*, **62**, 57–66.

Cerny, P., Novak, M., Chapman, R. and Ferreira, K.J. (2007) Subsolidus behavior of niobian rutile from the Pisek region, Czech Republic: a model for exsolution in W- and $Fe^{2+} >> Fe^{3+}$-rich phases. *Journal of Geosciences*, **52**, 143–159.

Chakhmouradian, A.R., Mitchell, R.H., Burns, P.C. and Mikhailova, Y. (2008) Marianoite, a new member of the cuspidine group from the Prairie Lake silicocarbonatite, Ontario. *The Canadian Mineralogist*, **46**, 1023–1032.

Christiansen, C.C., Johnsen, O. and Makovicky, E. (2003*a*) Crystal chemistry of the rosenbuschite group. *The Canadian Mineralogist*, **41**, 1203–1224.

Christiansen, C.C., Gault, R.A., Grice, J.D. and Johnsen, O. (2003*b*) Kochite, a new member of the rosenbuschite group from the Werner Bjerge alkaline complex, East Greenland. *European Journal of Mineralogy*, **15**, 551–554.

Clark, J.R. and Williams-Jones, A.E. (2004) *Rutile as a potential indicator mineral for metamorphosed metallic ore deposits*. Rapport Final de DIVEX, Sous-project SC2, Montréal, Canada, 17 pp.

Comin-Chiaramonti, P. and Gomes, C.B. (2005) *Mesozoic to Cenozoic Alkaline Magmatism in the Brazilian Platform*. FAPESP, São Paulo, Brazil, 751 pp.

Cucciniello, C., Tucker, R.D., Jourdan, F., Melluso, L. and Morra, V. (2016) The age and petrogenesis of the alkaline magmatism of Ampasindava Peninsula and Nosy Be archipelago, northern Madagascar. *Mineralogy and Petrology*, **110**, 309–331.

Czamanske, G.K. and Dillet, B. (1988) Alkali amphibole, tetrasilicic mica and sodic pyroxene in peralkaline siliceous rocks, Questa caldera, New Mexico. *American Journal of Science*, **288-A**, 358–392.

De La Roche, H., Leterrier, P., Grandclaude, P. and Marchal, E. (1980) A classification of volcanic and plutonic rocks using R_1-R_2 diagram and major element analyses. Its relationships with current nomenclature. *Chemical Geology*, **29**, 183–210.

Enrich, G.E.R., Azzone, R.G., Ruberti, E., Gomes, C.B. and Comin-Chiaramonti, P. (2005) Itatiaia, Passa Quatro and São Sebastião Island, the major alkaline syenitic complexes from the Serra do Mar Region. Pp. 419–441 in: *Mesozoic to Cenozoic Alkaline Magmatism in the Brazilian Platform* (P. Comin-Chiaramonti and C.B. Gomes, editors). FAPESP, São Paulo, Brazil.

Enrich, G.E.R., Ruberti, E. and Gomes, C.B. (2009) Geology and geochronology of Monte de Trigo island alkaline suite, southeastern Brazil. *Revista Brasileira de Geociencias*, **39**, 67–80.

Fedele, L., Lustrino, M., Melluso, L., Morra, V., Zanetti, A. and Vannucci, R. (2015) Trace element distribution in plagioclase, alkali feldspar, Ti-magnetite, biotite and apatite in evolved potassic liquids from Campi Flegrei (Southern Italy). *American Mineralogist*, **100**, 233–249.

Foland, K.A., Landoll, J.D., Henderson, C.M.B. and Chen, J.-F. (1993) Formation of cogenetic quartz and nepheline syenites. *Geochimica et Cosmochimica Acta*, **57**, 697–704.

Geraldes, M.C., Motoki, A., Costa, A., Mota, C.E. and Mohriak, W.U. (2013) Geochronology (Ar/Ar and K/Ar) of the South Atlantic post-break-up magmatism. Pp. 41–74 in: *Conjugate Divergent Margins* (W.U. Mohriak, A. Danforth, P.J. Post, D.E. Brown, G.C. Tari, M. Nemčok, S.T. Sinha, editors). Geological Society, London, Special Publications, **369**.

Giehl, C., Marks, M.A.W. and Nowak, M. (2013) Phase relations and liquid lines of descent of an iron-rich peralkaline phonolitic melt: an experimental study. *Contributions to Mineralogy and Petrology*, **165**, 283–304.

Giret, A., Bonin, B. and Leger, J.M. (1980) Amphibole compositional trends in oversaturated and undersaturated alkaline plutonic ring-complexes. *The Canadian Mineralogist*, **18**, 481–495.

Gomes, C.B., Barbieri, M., Beccaluva, L., Brotzu, P., Conte, A., Garbarino, C., Macciotta, G., Melluso, L., Morbidelli, L., Ruberti, E., Scheibe, L.F., Tamura, R. M. and Traversa, G. (1987) Petrological and geochemical studies of alkaline rocks from continental Brazil. 2. The Tunas massif, state of Paraná. *Geochimica Brasiliensis*, **1**, 201–234.

Gomes, C.B., Ruberti, E., Comin-Chiaramonti, P. and Azzone, R. (2011) Alkaline magmatism in the Ponta Grossa Arch, SE Brazil: a review. *Journal of South American Earth Sciences*, **32**, 152–168.

Gualda, G. and Vlach, S.R.F. (2007) The Serra da Graciosa A-type granites and syenites, southern Brazil part 3: magmatic evolution and post-magmatic breakdown of amphiboles of the alkaline association. *Lithos*, **93**, 328–339.

Guarino, V., Fedele, L., Franciosi, L., Lonis, R., Lustrino, M., Marrazzo, M., Melluso, L., Morra, V., Rocco, I.

https://doi.org/10.1180/minmag.2016.080.122 Published online by Cambridge University Press

and Ronga, F. (2011) Mineral compositions and magmatic evolution of the calcalkaline rocks of northwestern Sardinia, Italy. *Periodico di Mineralogia*, **80**, 517–545.

Guarino, V., Azzone, R.G., Brotzu, P., Gomes, C.B., Melluso, L., Morbidelli, L., Ruberti, E., Tassinari, C. C.G. and Brilli, M. (2012) Magmatism and fenitization at the Ipanema mafic-ultramafic alkaline-carbonatitic complex, São Paulo State, Brazil. *Mineralogy and Petrology*, **104**, 43–61.

Guarino, V., Wu, F.-Y., Lustrino, M., Melluso, L., Brotzu, P., Gomes, C.B., Ruberti, E., Tassinari, C.C.G. and Svisero, D.P. (2013) U-Pb ages, Sr-Nd- isotope geochemistry and petrogenesis of kimberlites, kamafugites and phlogopite-picrites of the Alto Paranaíba Igneous Province, Brazil. *Chemical Geology*, **353**, 65–82.

Gupta, A.K. (2015) *Origin of Potassium-Rich Silica-Deficient Igneous Rocks.* Springer, 536 pp. ISBN: 978-81-322-2082-1

Hamilton, D.L. and MacKenzie, W.S. (1965) Phase equilibrium studies in the system $NaAlSiO_4$ (nepheline) –$KAlSiO_4$– (kalsilite)– SiO_2– H_2O. *Mineralogical Magazine*, **34**, 214–231.

Harris, C., Marsh, J.S. and Milner, S.C. (1999) Petrology of the alkaline core of the Messum Igneous Complex, Namibia: evidence for the progressively decreasing effect of crustal contamination. *Journal of Petrology*, **40**, 1377–1397.

Janasi, V. de A., de Freitas, V.A. and Heaman, L.H. (2011) The onset of flood basalt volcanism, northern Parana basin, Brazil: a precise U-Pb baddeleyite/zircon age for a Chapecó-type dacite. *Earth and Planetary Science Letters*, **302**, 147–153.

Kempe, U., Möckel, R., Graupner, T., Kynicky, J. and Dombon, E. (2015) The genesis of Zr-Nb-REE mineralisation at Khalzan Buregte (Western Mongolia) reconsidered. *Ore Geology Reviews*, **64**, 602–625.

Lanyon, R. and le Roex, A.P. (1995) Petrology of the alkaline and ultramafic lamprophyres associated with the Okenyenya igneous complex, northwestern Namibia. *South African Journal of Geology*, **98**, 140–156.

Leake, B.E., Woolley, A.R., Arps, C.E.S., Gilbert, M.C., Grice, J.D., Hawthorne, F.C., Kato, A., Kisch, A.J., Krivovichev, V.G., Linthout, K., Laird, J., Mandarino, J.A., Maresch, W.V., Nickel, E.H., Schumacher, J.C., Smith, D.C., Stephenson, N.C.N., Whittaker, E.J.W. and Youzhi, G. (1997) Nomenclature of amphiboles: report of the subcommittee on amphiboles of the International Mineralogical Association, commission on new minerals and minerals names. *The Canadian Mineralogist*, **35**, 219–246.

Le Maitre, R.W. (2002) *Igneous Rocks: a Classification and Glossary of Terms: Recommendations of the International Union of Geological Sciences Subcommission on the Systematics of Igneous Rocks.* Cambridge University Press, Cambridge, UK, 236 pp.

Lustrino, M., Dallai, L., Giordano, R., Gomes, C.B., Melluso, L., Morbidelli, L., Ruberti, E. and Tassinari, C.C.G. (2003) Geochemical and Sr-Nd-O Isotopic features of the Poços de Caldas alkaline massif (SP-MG, SE Brazil): relationships with the Serra do Mar analogues. Pp. 593–595 in: *IV South American Symposium on Isotope Geology.* Short Papers. Salvador-BA, Brazil.

Lustrino, M., Melluso, L., Brotzu, P., Gomes, C.B., Morbidelli, L., Muzio Sauer, R., Ruberti, E. and Tassinari, C.C.G. (2005) Petrogenesis of the Early Cretaceous Valle Chico igneous complex (SE Uruguay): relationships with Paraná-Etendeka felsic rocks. *Lithos*, **82**, 407–434.

Lustrino, M., Cucciniello, C., Melluso, L., Tassinari, C.C. G., dè Gennaro, R. and Serracino, M. (2012) Petrogenesis of Cenozoic volcanic rocks in the NW sector of the Gharyan volcanic field, Libya. *Lithos*, **155**, 218–235.

Lyubetskaya, T. and Korenaga, J. (2007) Chemical composition of Earth's primitive mantle and its variance: 1. *methods and results. Journal of Geophysical Research*, **112**, B03211. https://doi.org/10.1019/2005JB004223

Macdonald, R. and Belkin, H.E. (2002) Compositional variation in minerals of the chevkinite group. *Mineralogical Magazine*, **66**, 1075–1098.

Macdonald, R., Bagiński, B., Dzierżanowski, P., Fettes, D.J. and Upton, B.G.J. (2013*a*) Chevkinite-group minerals in UK Paleogene granites: underestimated REE-bearing accessory phases. *The Canadian Mineralogist*, **51**, 333–347.

Macdonald, R., Bagiński, B., Dzierżanowski, P. and Jokubauskas, P. (2013*b*) Apatite-supergroup minerals in UK Palaeogene granites: composition and relationship to host-rock composition. *European Journal of Mineralogy*, **25**, 461–471.

Marks, M.A.W., Coulson, I.M., Schilling, J., Jacob, D.E., Schmitt, A.K. and Markl, G. (2008) The effect of titanite and other HFSE-rich mineral (Ti-andradite, zircon, eudialyte) fractionation on the geochemical evolution of silicate melts. *Chemical Geology*, **257**, 153–172.

Marks, M.A.W., Hettmann, K., Schilling, J., Frost, B.R. and Markl, G. (2011) The mineralogical diversity of alkaline igneous rocks: critical factors for the transition from miaskitic to agpaitic phase assemblages. *Journal of Petrology*, **52**, 439–455.

Mbouwou, G.I.B., Botelho, N. F., Lagmet, C.A. and Ngounouno, I. (2015) Petrology of peraluminous and peralkaline rhyolites from the SE Lake Chad (northernmost Cameroon Line). *Journal of African Earth Sciences*, **112**, 129–141.

https://doi.org/10.1180/minmag.2016.080.122 Published online by Cambridge University Press

Meinhold, G. (2010) Rutile and its application in Earth Sciences. *Earth-Science Reviews*, **102**, 1–28.

Melluso, L., Lustrino, M., Ruberti, E., Brotzu, P., Gomes, C.B., Morbidelli, L., Morra,V., Svisero, D.P. and d'Amelio, F. (2008) Major and trace element composition of olivine, perovskite, clinopyroxene, Cr-Fe-Ti oxides, phlogopite and host kamafugites and kimberlites, Alto Paranaíba, Brazil. *The Canadian Mineralogist*, **46**, 19–40.

Melluso, L., Srivastava, R.K., Guarino, V., Zanetti, A. and Sinha, A.K. (2010) Mineral compositions and magmatic evolution of the Sung Valley ultramafic-alkaline-carbonatitic complex (NE India). *The Canadian Mineralogist*, **48**, 205–229.

Melluso, L., de' Gennaro, R., Fedele, L., Franciosi, L. and Morra, V. (2012*a*) Evidence of crystallization in residual, Cl-F-rich, agpaitic, trachyphonolitic magmas and primitive Mg-rich basalt-trachyphonolite interaction in the lava domes of the Phlegrean Fields (Italy). *Geological Magazine*, **149**, 532–550.

Melluso, L., Srivastava, R.K., Petrone, C.M., Guarino, V. and Sinha, A.K. (2012*b*) Mineralogy, magmatic affinity and evolution of the Early Cretaceous alkaline complex of Jasra, Shillong Plateau, northeastern India. *Mineralogical Magazine*, **76**, 1099–1117.

Melluso, L., Hergt, J.M. and Zanetti, A. (2014*a*) The late crystallization stages of low-Ti, low-Fe tholeiitic magmas: insights from evolved Antarctic and Tasmanian rocks. *Lithos*, **188**, 72–83.

Melluso, L., Morra, V., Guarino, V., de' Gennaro, R., Franciosi, L. and Grifa, C. (2014*b*) The crystallization of shoshonitic to peralkaline trachyphonolitic magmas in a H_2O-Cl-F- rich environment at Ischia (Italy), with implications for the feeder system of the Campania Plain volcanoes. *Lithos*, **210–211**, 242–259.

Menezes, S.G., Azzone, R.G., Rojas, G.E.E., Ruberti, E., Cagliarani, R., Gomes, C.B. and Chmyz, L. (2015) The antecryst compositional influence on Cretaceous alkaline lamprophyre dykes, SE Brazil. *Brazilian Journal of Geology*, **45**, 79–93.

Mitchell, R.H. and Liferovich, R.P. (2004) Ecandrewsite-zincian pyrophanite from lujavrite, Pilanesberg alkaline complex, South Africa. *Mineralogical Magazine*, **42**, 1169–1178.

Morbidelli, L., Gomes, C.B., Beccaluva, L., Brotzu, P., Conte, A.M., Ruberti, E. and Traversa, G. (1995) Mineralogical, petrological and geochemical aspects of alkaline and alkaline-carbonatite associations from Brazil. *Earth-Science Reviews*, **39**, 135–168.

Moreau, C., Ohnenstetter, D., Demaiffe, D. and Robineau, B. (1996) The Los Archipelago nepheline syenite ring structure: a magmatic marker of the evolution of the central and equatorial Atlantic. *The Canadian Mineralogist*, **34**, 281–299.

Motoki, A., Sichel, S.E., Vargas, T., Aires, J.R., Iwanuch, W., Mello, S.L.M., Motoki, K.F., Da Silva S., Balmant, A. and Gonçalves, J. (2010) Geochemical evolution of the felsic alkaline rocks of Tanguá and Rio Bonito intrusive bodies, State of Rio de Janeiro, Brazil. *São Paulo UNESP, Geociências*, **29**, 291–310.

Motoki, A., Sichel, S.E., Vargas, T., Melo, D.P. and Motoki, K.F. (2015) Geochemical behaviour of trace elements during fractional crystallization and crustal assimilation of the felsic alkaline magmas of the state of Rio de Janeiro, Brazil. *Anais da Academia Brasileira de Ciencias*, **87**, 1959–1979.

Olin, P.H. and Wolff, J.A. (2012) Partitioning of rare earth and high field strength elements between titanite and phonolitic liquid. *Lithos*, **128**, 46–54.

Penalva, F. (1967) Geologia e tectonica da região do Itatiaia. *Boletim Facultade Filosofia Ciências e Letras, Università de São Paulo*, **302**, 95–196.

Pires, G.L.C., Bongiolo, E.M., Nuemann, R. and Avila, C. A. (2014) Caracterizaçao petrografica e mineralogica de brechas magmatico-hidrotermais no complexo alcalino de Itatiaia, estado do Rio de Janeiro: ocorrencias de fluorita e minerais de ETR. *Anuario do Instituto de Geociencias, UFRJ*, **37**, 4–15.

Platt, R.G., Wall, F., Williams, C.T. and Woolley, A.R. (1987) Zirconolite, chevkinite and other rare earth minerals from nepheline syenites and peralkaline granites and syenites of the Chilwa alkaline province, Malawi. *Mineralogical Magazine*, **51**, 253–263.

Platt, R.G. and Woolley, A.R. (1988) The mafic mineralogy of the peralkaline syenites and granites of the Mulanje complex, Malawi. *Mineralogical Magazine*, **50**, 85–99.

Pouchou, J.L. and Pichoir, F. (1991) Quantitative analysis of homogeneous or stratified microvolumes applying the model "PAP". Pp. 31–75 in: *Electron Probe Quantitation* (K.F.J. Heinrich and D.E. Newbury, editors). Plenum Press, New York.

Renne, P.R., Ernesto, M., Pacca, I.G., Coe, R.S., Glen, J.M., Prevot, M. and Perrin, M. (1992) The age of Paraná flood volcanism, rifting of Gondwanaland, and the Jurassic-Cretaceous boundary. *Science*, **258**, 975–979.

Ryabchikov, I.D. and Kogarko L.N. (2006) Magnetite compositions and oxygen fugacities of the Khibina magmatic system. *Lithos*, **91**, 35–45.

Riccomini, C., Velazquez, V.F. and Gomes, C.B. (2005) Tectonic controls of the Mesozoic and Cenozoic alkaline magmatism in the central-southeastern Brazilian Platform. Pp. 31–55 in: *Mesozoic to Cenozoic Alkaline Magmatism in the Brazilian Platform* (P. Comin-Chiaramonti and C.B. Gomes, editors). FAPESP, São Paulo, Brazil.

Ridolfi, F., Renzulli, A., Macdonald, R. and Upton, B.G.J. (2006) Peralkaline syenite autoliths from Kilombe volcano, Kenya Rift Valley: evidence for subvolcanic interaction with carbonatitic fluids. *Lithos*, **91**, 373–392.

https://doi.org/10.1180/minmag.2016.080.122 Published online by Cambridge University Press

Ronga, F., Lustrino, M., Marzoli, A. and Melluso, L. (2010) Petrogenesis of a basalt-comendite-pantellerite rock suite: the Boseti volcanic complex, Main Ethiopian Rift. *Mineralogy and Petrology*, **98**, 227–243.

Rønsbo, J.G. (2008) Apatite in the Ilimaussaq alkaline complex: occurrence, zonation and compositional variation. *Lithos*, **160**, 71–82.

Rønsbo, J.G., Sørensen, H., Roda-Robles, E., Fontan, F. and Monchoux, P. (2014) Rinkite- nacareniobsite-(Ce) solid solution series and hainite from the Ilímaussaq alkaline complex: occurrence and compositional variation. *Bulletin of the Geological Society of Denmark*, **62**, 1–15.

Sauerzapf, U., Lattard, D., Burchard, M. and Engelmann, R. (2008) The titanomagnetite-ilmenite equilibrium: new experimental data and thermo-oxybarometric application to the crystallization of basic to intermediate rocks. *Journal of Petrology*, **49**, 1161–1185.

Schmitt, A.K., Emmermann, R., Trumbull, R.B., Buhn, B. and Henjes-Kunst F. (2000) Petrogenesis and ^{40}Ar-^{39}Ar geochronology of the Brandberg complex, Namibia: evidence for a major mantle contribution in metaluminous and peralkaline granites. *Journal of Petrology*, **41**, 1207–1239.

Sichel, S.E., Motoki, A., Iwanuch, W., Vargas, T., Aires, J. R., Pereira de Melo, D., Motoki, K.F., Balmant, A. and Rodrigues, J.G. (2012) Cristalização fracionada e assimilação da crosta continental pelos magmas de rochas alcalinas félsicas do estado do Rio de Janeiro, Brazil. *Anuário do Instituto de Geociências*, **35**, 84–104.

Sonoki, I.K. and Garda, G.M. (1988) Idades K-Ar de rochas alcalinas do Brasil Meridional e Paraguai oriental: compilaçao e adaptaçao às novas constantes de decaimento. *Boletim IG USP, Serie Cientifica*, **19**, 63–98.

Sørensen, H. (1997) The agpaitic rocks – an overview. *Mineralogical Magazine*, **61**, 485–498.

Spinelli, F.P. and Gomes, C.B. (2008) A occorrencia alcalina de Cananeia, litoral sul do estado de Sao Paulo: petrologia e geoquimica. *Revista Brasileira de Geociencias*, **39**, 304–323.

Thompson, R.N., Gibson, S.A., Mitchell, J.G., Dickin, A. P., Leonardos, O.H., Brod, J.A. and Greenwood, J.C. (1998) Migrating Cretaceous-Eocene magmatism in the Serra do Mar alkaline Province, SE Brazil: melts from the deflected Trindade mantle plume? *Journal of Petrology*, **39**, 1493–1526.

Troll, V.R., Sachs, P.M., Schmincke, H.-U. and Sumita, M. (2003) The REE-Ti mineral chevkinite in comenditic magmas from Gran Canaria, Spain: a SYXRF-probe study. *Contributions to Mineralogy and Petrology*, **145**, 730–741.

Tupinambá, M., Heilbron, M., Valeriano, C., Porto Junior, R., Blanco de Dios F., Machado, N., Silva, L.G.E. and Horta de Almeida, J.C. (2012) Juvenile contribution of the Neoproterozoic Rio Negro Magmatic Arc (Ribeira Belt, Brazil): implications for Western Gondwana amalgamation. *Gondwana Research*, **21**, 422–438.

Turner, S., Regelous, M., Kelley, S., Hawkesworth, C.J. and Mantovani, M.S.M. (1994) Magmatism and continental break-up in the South Atlantic: High precision ^{40}Ar-^{39}Ar geochronology. *Earth and Planetary Science Letters*, **121**, 333–348.

Ulbrich, H.H.G.J. and Gomes, C.B. (1981) Alkaline igneous rocks from continental Brazil. *Earth-Science Reviews*, **17**, 135–154.

Valença, J.G. (1980) *Geology, petrography and petrogenesis of some alkaline igneous complexes of Rio de Janeiro State, Brazil*. PhD Thesis, University of Western Ontario, Canada, 248 pp.

Vilalva, F.C.J., Vlach, S.R.F. and Simonetti, A. (2013) Nacareniobsite-(Ce) and britholite-(Ce) in peralkaline granites from the Morro Redondo complex, Graciosa Province, Southern Brazil: occurrence and compositional data. *The Canadian Mineralogist*, **51**, 313–332.

Vlach, S.R.F. and Gualda, G. (2007) Allanite and chevkinite in A-type granites and syenites of the Graciosa Province, southern Brazil. *Lithos*, **97**, 98–121.

Woolley, A.R. and Platt, R.G. (1986) The mineralogy of nepheline syenite complexes from the northern part of the Chilwa Province, Malawi. *Mineralogical Magazine*, **50**, 597–610.

Woolley, A.R. and Platt, R.G. (1988) The peralkaline nepheline syenites of the Junguni intrusion, Chilwa province, Malawi. *Mineralogical Magazine*, **52**, 425–433.

Xirouchakis, D. and Lindsley, D.H. (1998) Equilibria among titanite, hedenbergite, fayalite, quartz, ilmenite, and magnetite: experiments and internally consistent thermodynamic data for titanite. *American Mineralogist*, **83**, 712–725.

https://doi.org/10.1180/minmag.2016.080.122 Published online by Cambridge University Press